A Coordinated Energy Management Framework for Industrial, Residential and Commercial Energy Hubs considering Demand Response Programs

Seyed Amir Mansouri [1], Mohammad Sadegh Javadi [2*], Amir Ahmarinejad [3], Emad Nematbakhsh [4], Abbas Zare [5] and Joao P. S. Catalao [2,6]

[1] Department of Electrical Engineering, Yadegar-e-Imam Khomeini (RAH) Shahre Rey Branch, Islamic Azad University, Tehran, Iran
[2] Institute for Systems and Computer Engineering, Technology and Science (INESC TEC), Porto, Portugal
[3] Department of Electrical Engineering, Central Tehran Branch, Islamic Azad University, Tehran, Iran
[4] Faculty of Electrical Engineering, University of Isfahan, Isfahan, Iran
[5] Department of Electrical, Electronic, and Information Engineering, University of Bologna, Bologna, Italy
[6] Faculty of Engineering of the University of Porto, Porto, Portugal

Abstract

This paper proposes an energy hub management model for residential, commercial, and industrial hubs, considering demand response programs (DRPs). The network configuration and AC optimal power flow (ACOPF) constraints have been applied to the model to prevent any unreal power transaction in the system. The cost due to environmental emissions has also been taken into account and the problem is modeled as a dynamic optimization problem, solved using the CPLEX solver in the GAMS software, interfaced with MATLAB/MATPOWER for the power flow analysis. Besides, the problem is studied in two cases as coordinated and uncoordinated operation modes to investigate their impacts on the operating cost, emission, and power losses. The obtained results show that the coordinated operation would lead to reducing the operating cost, power losses, and emission. Moreover, the impacts of the coordinated and uncoordinated operation modes on the load demand-supply under contingent events and disconnection from the upstream grid are assessed. The results derived from the simulation verify the superior performance of the coordinated operation. It is also noted that the DRP leads to mitigating the operating costs.

Keywords: Energy Hub, Energy Management, Demand Response Programs, Renewable Energy Resources, Electric Vehicles, AC Optimal Power Flow.

* Corresponding Author: msjavadi@gmail.com

Nomenclature

Abbreviations

CHP	Combined heat and power
EH	Electrical heater
EHP	Electrical heat pump
AC	Absorbed chiller
EES	Electrical energy storage
TES	Thermal energy storage

Indices

t	Time index
s	Season index
sc	Scenario index
em	Emission type index
k	Energy hub index
i	Energy hub type index
l	Line index
m,n	Index of nodes

Scalars

ρ_{sc}	The probability of each scenario
ω_s	The number of days at each season
Δt	Time slot (h)
η^{T}	Transformer electricity efficiency (%)
$\eta_P^{CHP} / \eta_H^{CHP}$	CHP electrical/ heating efficiency (%)
η^{Boiler}	Boiler efficiency (%)
η^{EH}	EH efficiency (%)
$\eta_H^{EHP} / \eta_C^{EHP}$	EHP heating/cooling efficiency (%)
$\eta_{Ch}^{EES} / \eta_{Dis}^{EES}$	EES charging/discharging efficiency (%)
η^{AC}	Absorption chiller efficiency (%)
λ_{em}	Emission cost ($/kg)
λ^{EES}	EES operation cost ($/kW)
λ^{TES}	TES operation cost ($/kW)
$P^{EES,Ch.,Max} / P^{EES,Dis.,Max}$	Max charging/discharging rate of EES (kW)
$P^{TES,Ch.,Max} / P^{TES,Dis.,Max}$	Max charging/discharging rate of TES (kW)
$P^{Min,CHP} / P^{Max,CHP}$	Min/Max electrical power of CHP (kW)
$H^{Min,CHP} / H^{Max,CHP}$	Min/Max thermal power of CHP (kW)
$Cap^{Min,Boiler} / Cap^{Max,Boiler}$	Min/Max Boiler capacity (kW)
$Cap^{Min,EH} / Cap^{Max,EH}$	Min/Max EH capacity (kW)
$Cap^{Min,EHP} / Cap^{Max,EHP}$	Min/Max EHP capacity (kW)
$Cap^{Min,AC} / Cap^{Max,AC}$	Min/Max AC capacity (kW)
$Cap^{Min,EES} / Cap^{Max,EES}$	Min/Max EES capacity (kW)
$Cap^{Min,CHP} / Cap^{Max,CHP}$	Min/Max CHP capacity (kW)

G_0^a	Irradiation of sun at the standard condition (W/m^2)
$P_{k_i}^{PV,Max}$	Maximum power of solar panel at the standard condition (kW)
$\mu_{P\max}$	Thermal sensitivity of solar panel (kW/C^o)
$NOCT$	Normal operating temperature of the solar panel (C^o)
$T_{M,0}$	solar panel temperature at the standard condition (C^o)
$p_{k_i}^r$	Wind turbine nominal power (kW)
$v_{ci}/v_{co}/v_r$	Cut-in/Cut-out and rated speed of wind turbine (m/s)
Parameters	
N_t	The number of operating hours
N_S	The number of seasons
N_{sc}	The number of scenarios
$\lambda_{k_i,s,t}^{Buy}$	Price of buying electrical power ($/kWh)
$\lambda_{k_i,s,t}^{Sell}$	Price of Selling electrical power ($/kWh)
$\lambda_{k_i,s}^{DR}$	Operation cost of DR programs ($/kW)
$\lambda_{k_i,s}^{ENS}$	Penalty price for ENS ($/kWh)
$\lambda_{k_i,s,t}^{Gas}$	Gas price ($/kWh)
EF_{em}^G	Emission factor for up-stream grid (kg/kW)
EF_{em}^{CHP}	Emission factor for CHP (kg/kW)
EF_{em}^B	Emission factor for Boiler (kg/kW)
$G_{sc,s,t}^a$	Irradiation of sun (W/m^2)
$\alpha_{k_i}^{initial}$	Initial state of charge of the EES/TES (%)
$T_{sc,s,t}^a$	Air temperature (C^o)
$v_{sc,s,t}^w$	Wind speed (m/s)
$P_{k_i,sc,s,t}^{EL}$	Electrical demand (kW)
$H_{k_i,sc,s,t}^{HL}$	Heating demand (kW)
$C_{k_i,sc,s,t}^{CL}$	Cooling demand (kW)
Variables	
TOC	Total operation cost
$P_{k_i,sc,s,t}^{G\to H}$	Transferred power from up-stream grid to energy hub (kW)
$P_{k_i,sc,s,t}^{M\to H}/P_{k_i,sc,s,t}^{H\to M}$	Transferred power between energy hubs (kW)
$P_{k_i,sc,s,t}^{H\to G}$	Transferred power from energy hub to up-stream grid (kW)
$P_{k_i,sc,s,t}^{(.)\to(.)}$	Electrical power flow between assets (kW)
$H_{k_i,sc,s,t}^{(.)\to(.)}$	Heating power flow between assets (kW)
$C_{k_i,sc,s,t}^{(.)\to(.)}$	Cooling power flow between assets (kW)
$f_{k_i,sc,s,t}^{CHP}$	CHP fuel cost ($)
$f_{k_i,sc,s,t}^{Boiler}$	Boiler fuel cost ($)
$f_{k_i,sc,s,t}^{EES}$	EES operation cost ($)

$f_{k_i,sc,s,t}^{TES}$	TES operation cost ($)
$P_{k_i,sc,s,t}^{ENS}$	Energy not served (kW)
$P_{k_i,sc,s,t}^{CHP}$	Electrical power of CHP (kW)
$H_{k_i,sc,s,t}^{CHP}$	Thermal power of CHP (kW)
$H_{k_i,sc,s,t}^{Boiler}$	Thermal power of Boiler (kW)
$P_{k_i,sc,s,t}^{EES,Ch.} / P_{k_i,sc,s,t}^{EES,Dis.}$	Charging/Discharging power of EES (kW)
$P_{k_i,sc,s,t}^{TES,Ch.} / P_{k_i,sc,s,t}^{TES,Dis.}$	Charging/Discharging power of TES (kW)
$P_{k_i,sc,s,t}^{EH} / H_{k_i,sc,s,t}^{EH}$	Electrical /Thermal power of EH (kW)
$P_{k_i,sc,s,t}^{EHP} / H_{k_i,sc,s,t}^{EHP} / C_{k_i,sc,s,t}^{EHP}$	Electrical /Heating/Cooling power of EHP (kW)
$H_{k_i,sc,s,t}^{AC} / C_{k_i,sc,s,t}^{AC}$	Heating /Cooling power of AC (kW)
$E_{k_i,sc,s,t}^{EES}$	Stored Energy in EES (kWh)
$E_{k_i,sc,s,t}^{TES}$	Stored Energy in TES (kWh)
$P_{k_i,sc,s,t}^{PV}$	Available photovoltaic power (kW)
$P_{k_i,sc,s,t}^{Wind}$	Available wind power (kW)
Decision Variables	
$I_{k_i,sc,s,t}^{CHP}$	Indicator of CHP operation
$I_{k_i,sc,s,t}^{Boiler}$	Indicator of Boiler operation
$I_{k_i,sc,s,t}^{EH}$	Indicator of EH operation
$I_{k_i,sc,s,t}^{EHP,C} / I_{k_i,sc,s,t}^{EHP,H}$	Indicator of EHP operation in cooling/heating mode
$I_{k_i,sc,s,t}^{AC}$	Indicator of AC operation
$I_{k_i,sc,s,t}^{EES,Ch.} / I_{k_i,sc,s,t}^{EES,Dis.}$	Indicator of EES operation in charging/discharging mode
$I_{k_i,sc,s,t}^{TES,Ch.} / I_{k_i,sc,s,t}^{TES,Dis.}$	Indicator of TES operation in charging/discharging mode

1- Introduction

1-1 Motivation

Today, natural gas networks are almost available everywhere. Therefore, the required conditions for the integrated operation of natural gas and electricity networks for the sake of supplying electrical, heating, and cooling load demands in residential, commercial, and industrial sectors are already met. Such energy systems with multiple energy carriers are known as “energy hub” [1]. These energy networks not only enhance the power system reliability and stability but also lead to reducing the operating costs compared to the individual operation [2]. Recently, several hubs with energy transaction capability are being operated integratedly by system operators, mainly thanks to the increased flexibility of consumers in power markets. Such a system is called “smart energy

hub", equipped with smart sensors and it has access to the real-time data of the system for the coordinated operation [3–5]. The constraints of gas, electricity and heating systems have also been taken into consideration recently, to develop a close-to-real operation model [6]. This paper proposed a mixed-integer linear programming (MILP) model for the integrated operation of three residential, commercial, and industrial energy hubs. These hubs are connected to the IEEE 33-bus distribution system with the power transaction capability. Furthermore, the impacts of climate conditions on the load demand, renewable power generation, and electricity price have been studied using seasonal data over the year. The presented model incorporates the network constraints and power flow of lines to avoid any unreal power transaction. Moreover, a price-based demand response program (DRP) has been evaluated within the developed framework.

1-2 Literature review

Numerous research works have thus far been carried out to promote the energy hubs to smarter, more sustainable, and economically friendly hubs. In this respect, Ref. [7] presents a model for the operation of a group of energy hubs, aimed at mitigating the total operating cost and emission. A cost-benefit analysis has been done in Ref. [8] to optimally size the assets of a residential energy hub using reinforcement learning (RL). Ref. [9] studied the optimal operation of five energy hubs within a smart grid, aimed at minimizing the total operating cost and emission. The findings of this paper show that the coordinated operation of commercial and residential energy hubs with power transaction capability results in improved efficiency, reduced operating cost, and alleviated emission. The optimal operation of energy hubs, integrated with a smart hub has been investigated by employing the Stackelberg game in [10], taking into account DRPs and gas dispatch factor. The model is designed in a way to maximize the profit of the smart energy hub and consumers simultaneously. A multi-objective scheduling model has been suggested in [11] for smart hubs in the presence of shiftable loads. The objectives include minimizing the total operating cost, emission, and voltage deviation. A hierarchical operation model has been developed in [12] for multiple energy hubs in neighboring grids. The model aims to maximize the profit of the central hub and shave the peak load of the upstream grid. The obtained results show 9.4% reduction in the energy supply cost and 4.55% increase in the profit of hubs. A risk-oriented scenario-based stochastic programming is presented in [13] for the optimal operation of a smart energy hub. In this respect, the conditional value-at-risk (CVaR) measure has been utilized for the risk

assessment. The objective function is the weighted sum of the operating cost and emission. Ref. [14] proposes an energy management model for the modern smart buildings, integrated with energy systems. The simulation results indicate that the integration of the electric and heating systems of such buildings with a heat pump would result in 27% savings in the total energy cost. The application of energy management system for smart homes in the presence of different energy tariffs has been presented in [15]. The integrated DRPs in multi-energy systems have been studied in [16], where the modeling, operational strategy, and market behavior have been analyzed. A novel energy management model has been suggested in [17] for a system, including ten smart energy hubs with integrated demand-side management. Employing the mentioned model has resulted in reducing the expected cost and peak electrical demand. A multi-objective optimization framework has been developed in Ref. [18] for the energy scheduling problem of an 83-bus distribution system. The model includes a demand-side management strategy in the presence of distributed renewable energies sources (RESs), including wind energy and solar energy as well as electrical energy storage (EES) systems. Besides, the objectives of the model are total operating cost minimization, minimization of loss of load expectation (LOLE), and minimizing the deviation between the demand curve and power output of RESs. Ref. [19] presented a CVaR-constrained scheduling model for a smart energy hub, equipped with compressed air energy storage (CAES) systems, and DRPs. It is noteworthy that the uncertainties caused by the wind power generation and load demand are characterized using the Monte-Carlo simulation (MCS). Ref. [20] developed an innovative energy management framework for the cooperative operation management framework using a MILP technique, solved using the CPLEX solver in the GAMS software. The obtained results show the reduction in the load demand, emission, and operating cost of the system. An energy management model has been designed in [21] for a smart community in the presence of solar photovoltaic (PV) systems and user-dominated demand-side response. The model considers a local energy pool to activate the peer-to-peer (P2P) transactions. Furthermore, the electricity in the local pool market is real-time and dependent upon the demand/supply ratio. The results confirm that the profit of customers in the energy pool with PV units would be higher than the case without PV systems. The flexibility of the multi-energy systems has been utilized in [22] to mitigate the wind power generation uncertainty, which in turn results in increasing the profit.

Recently, many studies have proposed energy management frameworks based on dynamic programming. For instance, Ref. [23] presents a two-stage supervisory strategy considering DRPs

and consumers' thermal comfort. The results of this study illustrate that the proposed model not only reduces operating costs but also guarantees thermal comfort. In [24] to enhance the resilience of a PV-based microgrid, an EES management model is proposed. The model is linearly formulated and its strength is to determine the optimal point between operating costs and system resilience. Ref. [25] presents rule-based demand management in microgrids considering real-time weather changes. The problem is solved by the closed-loop optimization method and the results prove the effectiveness of the proposed model. Ref. [26] presents a two-stage energy management framework to evaluate the impact of the presence of plug-in EVs and DRPs on operating results. In order to model price uncertainty, the CVaR method has been utilized and the results demonstrate that the use of plug-in EVs in microgrids is not only Reduces operating costs but also increases environmental sustainability.

1-3 Contribution

This paper presents an operation model for three residential, commercial, and commercial energy hubs. The model includes the DRP and renewable power generation, both wind and solar energies. Furthermore, the network constraints and AC optimal power flow (ACOPF) constraints have been applied to avoid any unreal power transaction in the system. The environmental issues have also been considered through SO_2, NO_2, and CO_2 emissions. The presented problem is formulated in a MILP framework and solved using the CPLEX solver in the GAMS software, interfaced with MATLAB/MATPOWER for the power flow calculations. The main contributions of the paper can be briefly stated as follows:

- Proposing an MILP model for coordinated power transactions between energy hubs
- Residential, commercial and industrial hubs are considered in the model
- Considering the ACOPF constraints to prevent any unreal power transaction
- Investigating the impacts of coordinated and uncoordinated operation modes on the operating cost, power losses, and emission.
- Investigating the effects of coordinated and uncoordinated operation modes on the load demand-supply during contingent events.
- Analyzing the impact of DRPs on operating costs.

1-4- Organization of the paper

The paper is organized as follows where Section 2 presents the descriptions of different parts of the system. The problem is modeled in Section 3 and Section 4 represents the conceptual flowchart of the presented framework. Simulation results are proposed and discussed in Section 5. Lastly, some concluding remarks are included in Section 6.

2- System description

The system used in this paper includes three residential, commercial, and industrial hubs, connected to the IEEE 33-bus radial distribution system. As Fig. 1 depicts, the residential and commercial energy hubs are equipped with solar PV systems, while the industrial energy hub owns a wind turbine. Moreover, the industrial hub includes a parking lot for electric vehicles (EVs) of the employees so that the EVs can be utilized over peak load intervals. This figure shows the energy trading between energy hubs. As can be observed in Fig. 1(a), hubs can transact power with each other and also purchase power from the upstream grid. Using the uncoordinated operation mode deprives the energy hubs from power transaction with each other. In this case, hubs are only allowed to transact power with the upstream grid.

Fig. 1 illustrates the configuration of the energy hubs. It is worth mentioning that the internal configuration and equipment of the hubs studied in this paper are similar. Fig. 2 shows that the inputs of each energy hub are electricity and natural gas. Besides, each hub is capable of supplying its electrical load demand using a combined heat and power (CHP) unit, a PV system or a wind turbine, power transaction with the upstream grid, and trading power with other hubs. The electrical demand of each energy hub includes electrical loads, an electric heater (EH), and an electric heat pump (EHP). The cooling load demand is supplied using the EHP and the absorption chiller (AC). A boiler, the CHP unit, the EH, and the EHP are supposed to supply the heating load demand, including the AC and other heating loads. There are also electrical energy storage (EES) and thermal energy storage (TES) systems.

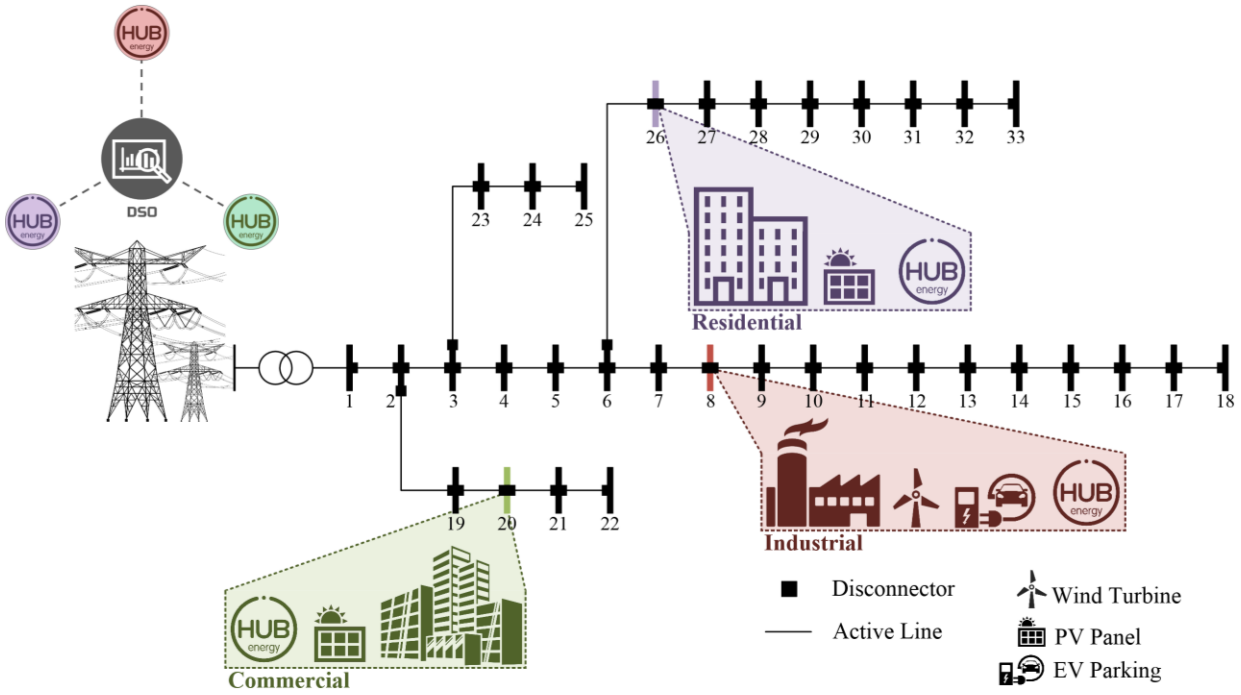

Fig. 1. The overview of the studied network.

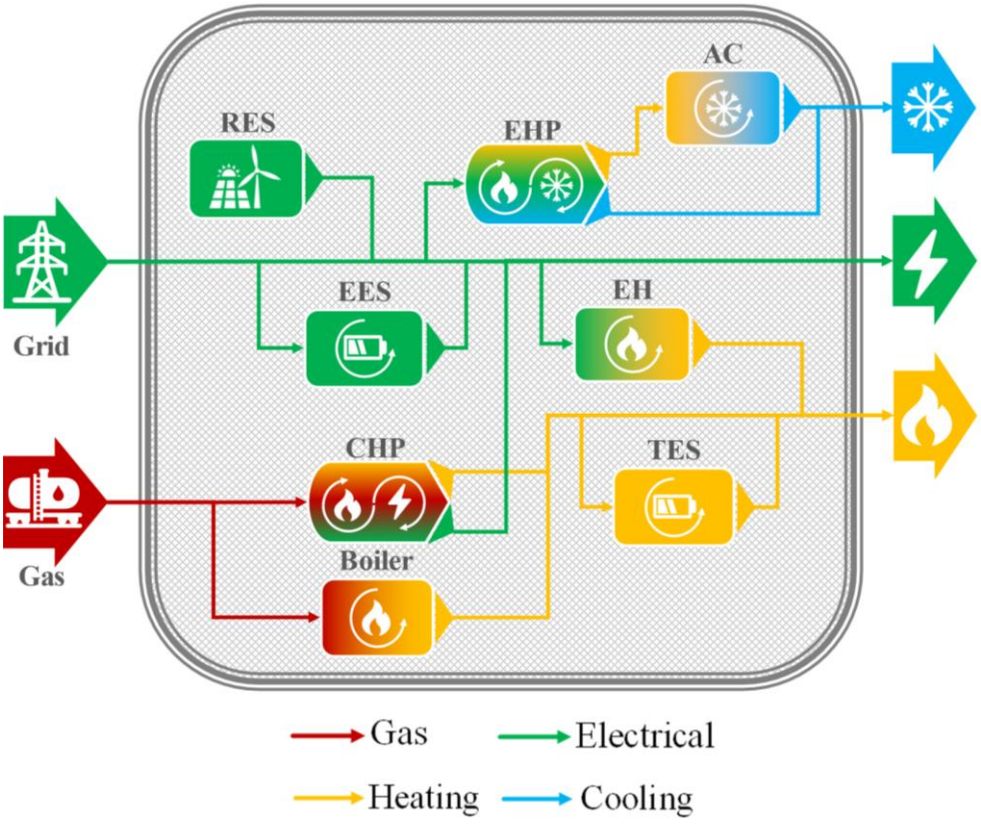

Fig. 2. Energy hub configuration.

3- Mathematical Formulation

- Objective function

The objective function of the problem is comprised of the operating cost of the CHP unit, boiler, storage system, power purchased from the upstream grid, and also costs, relating to the emission propagated by the CHP unit and the boiler. In addition, the energy not supplied (ENS) cost has also been taken into consideration [27]. The operating cost of the energy hub for a given day of a season is calculated as (1a), and it is multiplied by the number of days of each season to obtain the annual cost. The operating cost of the CHP unit and the boiler have been stated in (1b) and (1c) respectively [28], where $P_{k_i,sc,s,t}^{CHP}$ and $H_{k_i,sc,s,t}^{CHP}$ denote the electrical power and heat generated by the CHP unit of the hub *i* for season *s*, and time *t*, respectively. $\lambda_{k_i,s,t}^{Gas}$ is the price of the natural gas while η_P^{CHP} and η_H^{CHP} show the electrical and heat efficiencies of the CHP unit respectively [29–31].

$$Min: TOC = \sum_{sc}^{N_{sc}} \rho_{sc} \left\{ \sum_{s=1}^{N_s} \omega_s \sum_{t=1}^{N_T} \sum_{k_i \in K} \left[\begin{array}{l} \left(\dfrac{P_{k_i,sc,s,t}^{G\to H} \lambda_{k_i,s,t}^{Buy,G} + P_{k_i,sc,s,t}^{M\to H} \lambda_{k_i,s,t}^{Buy,M}}{\eta^T} \right) \Delta t - \left(P_{k_i,sc,s,t}^{H\to G} \lambda_{k_i,s,t}^{Sell,G} + P_{k_i,sc,s,t}^{H\to M} \lambda_{k_i,s,t}^{Sell,M} \right) \eta^T \Delta t \\ + f_{k_i,sc,s,t}^{CHP} + f_{k_i,sc,s,t}^{Boiler} + f_{k_i,sc,s,t}^{EES} + f_{k_i,sc,s,t}^{TES} + f_{ev,sc,s,t}^{EV} \\ + \sum_{em=1}^{EM} \lambda_{em} EF_{em}^{G} P_{k_i,sc,s,t}^{G\to H} + \lambda_{em} EF_{em}^{CHP} P_{k_i,sc,s,t}^{CHP} + \lambda_{em} EF_{em}^{B} H_{k_i,sc,s,t}^{Boiler} \\ + P_{k_i,sc,s,t}^{ENS} \lambda_{k_i,s}^{ENS} \Delta t \end{array} \right] \right\} \quad (1a)$$

Moreover, $H_{k_i,sc,s,t}^{Boiler}$ and η^{Boiler} are the heat generation and efficiency of the boiler respectively. $P_{k_i,sc,s,t}^{ENS}$ is the amount of ENS and $\lambda_{k_i,s}^{ENS}$ is the corresponding cost. As relationships (1d) and (1e) state, $f_{k_i,sc,s,t}^{EES}$ and $f_{k_i,sc,s,t}^{TES}$ indicate the operating cost of the EES and TES units, respectively, which are the functions of the charging and discharging rates and the related operating cost. $f_{ev,sc,s,t}^{EV}$ is the cost due to using the batteries of EVs. The cost of emission is a function of the power generation of the boiler and CHP units. EF_{em}^{CHP} and EF_{em}^{Boiler} are the emission coefficients of the CHP unit and boiler respectively. Lastly, $P_{k_i,sc,s,t}^{ENS}$ and $\lambda_{k_i,s}^{ENS}$ are the ENS cost and its corresponding costs. It should be noted that Δt is the time slot and it is supposed to be one hour in this study.

$$f_{k_i,sc,s,t}^{CHP} = \left(\frac{P_{k_i,sc,s,t}^{CHP}}{\eta_P^{CHP}} + \frac{H_{k_i,sc,s,t}^{CHP}}{\eta_H^{CHP}} \right) \lambda_{k_i,s,t}^{Gas} \Delta t \quad (1b)$$

$$f_{k_i,sc,s,t}^{Boiler} = \left(\frac{H_{k_i,sc,s,t}^{Boiler}}{\eta^{Boiler}} \right) \lambda_{k_i,s,t}^{Gas} \Delta t \quad (1c)$$

$$f_{k_i,sc,s,t}^{EES} = \lambda^{EES} \left(P_{k_i,sc,s,t}^{EES,Ch.} + P_{k_i,sc,s,t}^{EES,Dis.} \right) \quad (1d)$$

$$f_{k_i,sc,s,t}^{TES} = \lambda^{TES} \left(P_{k_i,sc,s,t}^{TES,Ch.} + P_{k_i,sc,s,t}^{TES,Dis.} \right) \quad (1e)$$

$$f_{ev,sc,s,t}^{EV} = \lambda^{EV} \left(P_{ev,sc,s,t}^{EV,Ch.} + P_{ev,sc,s,t}^{EV,Dis} \right) \quad (1f)$$

- **CHP model**

The constraints, relating to the CHP unit are presented using (2a)-(2c), where the binary variable $I_{k_i,sc,s,t}^{CHP}$ determines the OFF/ON status of the unit. If $I_{k_i,sc,s,t}^{CHP}$ is "1", it shows that the CHP unit is ON, otherwise it is OFF. $P^{Max,CHP}$ and $H^{Max,CHP}$ show the maximum power and heat generated by the CHP unit respectively [32]. Eqs. (2d) and (2e) state the electrical and heat energy balance equations.

$$Cap^{Min,CHP} I_{k_i,sc,s,t}^{CHP} \le P_{k_i,sc,s,t}^{CHP} + H_{k_i,sc,s,t}^{CHP} \le Cap^{Max,CHP} I_{k_i,sc,s,t}^{CHP} \quad (2a)$$

$$P^{Min,CHP} I_{k_i,sc,s,t}^{CHP} \le P_{k_i,sc,s,t}^{CHP} \le P^{Max,CHP} I_{k_i,sc,s,t}^{CHP} \quad (2b)$$

$$H^{Min,CHP} I_{k_i,sc,s,t}^{CHP} \le H_{k_i,sc,s,t}^{CHP} \le H^{Max,CHP} I_{k_i,sc,s,t}^{CHP} \quad (2c)$$

$$P_{k_i,sc,s,t}^{CHP} = P_{k_i,sc,s,t}^{CHP \to EL} + P_{k_i,sc,s,t}^{CHP \to EES} + P_{k_i,sc,s,t}^{CHP \to EHP} + P_{k_i,sc,s,t}^{CHP \to EH} + P_{k_i,sc,s,t}^{CHP \to M} + P_{k_i,sc,s,t}^{CHP \to G} + P_{k_i,sc,s,t}^{CHP \to EVs} \quad (2d)$$

$$H_{k_i,sc,s,t}^{CHP} = H_{k_i,sc,s,t}^{CHP \to HL} + H_{k_i,sc,s,t}^{CHP \to AC} + H_{k_i,sc,s,t}^{CHP \to TES} \quad (2e)$$

- **Boiler model**

Constraint (3a) states the limitations of the heat power generation by the boiler while the related capacity and the lower bound of the boiler capacity are shown by $Cap^{Max,Boiler}$ and $Cap^{Min,Boiler}$ respectively [33]. Besides, the binary variable $I_{k_i,sc,s,t}^{Boiler}$ determines that the boiler is ON or OFF. Eq. (3b) is the heat power balance of the boiler, showing that the heat generated by the boiler is consumed by the heat load demand and the AC or in case it is needed, it is stored by the TES.

$$Cap^{Min,Boiler} I_{k_i,sc,s,t}^{Boiler} \le H_{k_i,sc,s,t}^{Boiler} \le Cap^{Max,Boiler} I_{k_i,sc,s,t}^{Boiler} \quad (3a)$$

$$H_{k_i,sc,s,t}^{Boiler} = H_{k_i,sc,s,t}^{Boiler\to HL} + H_{k_i,sc,s,t}^{Boiler\to AC} + H_{k_i,sc,s,t}^{Boiler\to TES} \quad (3b)$$

- **EH model**

The constraint of the heat generation by the EH is shown in (4a). Eq. (4b) states the heat generated by the EH which is the product of the power input, $P_{k_i,sc,s,t}^{EH}$, and the efficiency of the system. As Eq. (4c) specifies, the electrical power required by the EH is supplied through the CHP unit, EES, PV system, upstream grid, or power transaction with other hubs [34]. Moreover, the heat generated by the EH unit is delivered only to the heating load demand.

$$Cap^{Min,EH} I_{k_i,sc,s,t}^{EH} \le H_{k_i,sc,s,t}^{EH} \le Cap^{Max,EH} I_{k_i,sc,s,t}^{EH} \quad (4a)$$

$$H_{k_i,sc,s,t}^{EH} = P_{k_i,sc,s,t}^{EH} \eta^{EH} \quad (4b)$$

$$P_{k_i,sc,s,t}^{EH} = P_{k_i,sc,s,t}^{G\to EH} + P_{k_i,sc,s,t}^{CHP\to EH} + P_{k_i,sc,s,t}^{EES\to EH} + P_{k_i,sc,s,t}^{RES\to EH} + P_{k_i,sc,s,t}^{M\to EH} + P_{k_i,sc,s,t}^{EVs\to EH} \quad (4c)$$

$$H_{k_i,sc,s,t}^{EH} = H_{k_i,sc,s,t}^{EH\to HL} + H_{k_i,sc,s,t}^{EH\to TES} \quad (4d)$$

- **EHP model**

The heating and cooling power generated by the EHP is limited as stated in (5a) and (5b), where $H_{k_i,sc,s,t}^{EHP}$ and $C_{k_i,sc,s,t}^{EHP}$ indicate the heating and cooling power generation of the EHP respectively. In addition, $I_{k_i,sc,s,t}^{EHP,H}$ and $I_{k_i,sc,s,t}^{EHP,C}$ are binary variables, relating to the heating and cooling modes of the EHP respectively. As inequality (5c) states, the EHP should operate in one of the mentioned modes at a time. The heating and cooling powers of the EHP are the functions of the electrical power input and the efficiency of the system in each mode. The electrical, heating, and cooling power balance equations of the EHP have been shown in (5f)-(5h) respectively.

$$Cap^{Min,EHP} I_{k_i,sc,s,t}^{EHP,H} \le H_{k_i,sc,s,t}^{EHP} \le Cap^{Max,EHP} I_{k_i,sc,s,t}^{EHP,H} \quad (5a)$$

$$Cap^{Min,EHP} I_{k_i,sc,s,t}^{EHP,C} \le C_{k_i,sc,s,t}^{EHP} \le Cap^{Max,EHP} I_{k_i,sc,s,t}^{EHP,C} \quad (5b)$$

$$H_{k_i,sc,s,t}^{EHP} = P_{k_i,sc,s,t}^{EHP} \eta_H^{EHP} \quad (5c)$$

$$H_{k_i,sc,s,t}^{EHP} = P_{k_i,sc,s,t}^{EHP} \eta_H^{EHP} \quad (5d)$$

$$C_{k_i,sc,s,t}^{EHP} = P_{k_i,sc,s,t}^{EHP} \eta_C^{EHP} \quad (5e)$$

$$P_{k_i,sc,s,t}^{EHP} = P_{k_i,sc,s,t}^{G\to EHP} + P_{k_i,sc,s,t}^{CHP\to EHP} + P_{k_i,sc,s,t}^{EES\to EHP} + P_{k_i,sc,s,t}^{RES\to EHP} + P_{k_i,sc,s,t}^{M\to EHP} + P_{k_i,sc,s,t}^{EVs\to EHP} \quad (5f)$$

$$H_{k_i,sc,s,t}^{EHP} = H_{k_i,sc,s,t}^{EHP\to HL} + H_{k_i,sc,s,t}^{EHP\to TES} \quad (5g)$$

$$C_{k_i,sc,s,t}^{EHP} = C_{k_i,sc,s,t}^{EHP\to CL} \quad (5h)$$

- **ACOPF constraints**

The cooling power generated by the AC is limited as shown in (6a) and the cooling power generation equation is indicated in (6b). Furthermore, Eqs. (6c) and (6d) are the heat power and cooling power balance equations respectively.

$$Cap^{Min,AC} I_{k_i,sc,s,t}^{AC} \le C_{k_i,sc,s,t}^{AC} \le Cap^{Max,AC} I_{k_i,sc,s,t}^{AC} \quad (6a)$$

$$C_{k_i,sc,s,t}^{AC} = H_{k_i,sc,s,t}^{AC} \eta^{AC} \quad (6b)$$

$$H_{k_i,sc,s,t}^{AC} = H_{k_i,sc,s,t}^{CHP\to AC} + H_{k_i,sc,s,t}^{Boiler\to AC} + H_{k_i,sc,s,t}^{TES\to AC} \quad (6c)$$

$$C_{k_i,sc,s,t}^{AC} = C_{k_i,sc,s,t}^{AC\to CL} \quad (6d)$$

- **EES model**

Constraint (7a) shows the limitation of the maximum energy that can be stored in the EES system. The energy balance equation of the EES system is stated in (7b), where the energy available in time interval *t* is a function of the energy available from the previous interval and the charging/discharging power at time *t*. The charging and discharging rates are limited by (7c) and (7d), where binary variables $I_{k_i,sc,s,t}^{EES,Ch}$ and $I_{k_i,sc,s,t}^{EES,Dis}$ determine the charging and discharging modes, respectively [35]. It is noteworthy that the EES system can operate only in one of the mentioned modes as shown in (7e) [36]. Moreover, the amount of energy stored in the EES system at the end of the scheduling period should be equal to that at the beginning of the scheduling period as expressed in (7f). The amount of the initial energy available in the EES system is shown in (7g). The charging and discharging power equations of the EES system are stated as (7h) and (7i) respectively [37].

$$Cap^{Min,EES} \le E_{k_i,sc,s,t}^{EES} \le Cap^{Max,EES} \quad (7a)$$

$$E_{k_i,sc,s,t}^{EES} = E_{k_i,sc,s,t-1}^{EES} + \left(P_{k_i,sc,s,t}^{EES,Ch.} \eta_{Ch}^{EES}\right)\Delta t - \left(\frac{P_{k_i,sc,s,t}^{EES,Dis.}}{\eta_{Dis}^{EES}}\right)\Delta t \quad (7b)$$

$$0 \le P_{k_i,sc,s,t}^{EES,Ch.} \le P^{EES,Ch.,Max} I_{k_i,sc,s,t}^{EES,Ch.} \quad (7c)$$

$$0 \le P_{k_i,sc,s,t}^{EES,Dis.} \le P^{EES,Dis.,Max} I_{k_i,sc,s,t}^{EES,Dis.} \quad (7d)$$

$$0 \le I_{k_i,sc,s,t}^{EES,Ch.} + I_{k_i,sc,s,t}^{EES,Dis.} \le 1 \quad (7e)$$

$$E_{k_i,sc,s,t=T}^{EES} = E_{k_i,sc,s,t=0}^{EES} \quad (7f)$$

$$E_{k_i,sc,s,t=0}^{EES} = \alpha_{k_i}^{initial} Cap^{Max,EES} \quad (7g)$$

$$P_{k_i,sc,s,t}^{EES,Ch.} = P_{k_i,sc,s,t}^{G\to EES} + P_{k_i,sc,s,t}^{CHP\to EES} + P_{k_i,sc,s,t}^{RES\to EES} + P_{k_i,sc,s,t}^{M\to EES} \quad (7h)$$

$$P_{k_i,sc,s,t}^{EES,Dis.} = P_{k_i,sc,s,t}^{EES\to EL} + P_{k_i,sc,s,t}^{EES\to G} + P_{k_i,sc,s,t}^{EES\to EHP} + P_{k_i,sc,s,t}^{EES\to EH} + P_{k_i,sc,s,t}^{EES\to M} \quad (7i)$$

- **TES model**

The relationships of the TES system are stated in (8a)-(8i) [37].

$$Cap^{Min,TES} \le E_{k_i,sc,s,t}^{TES} \le Cap^{Max,TES} \quad (8a)$$

$$E_{k_i,sc,s,t}^{TES} = E_{k_i,sc,s,t-1}^{TTES} + \left(H_{k_i,sc,s,t}^{TES,Ch}\eta_{Ch}^{TES}\right)\Delta t - \left(\frac{H_{k_i,sc,s,t}^{TES,Dis}}{\eta_{Dis}^{TES}}\right)\Delta t \quad (8b)$$

$$0 \le H_{k_i,sc,s,t}^{TES,Ch} \le H^{TES,Ch,Max} I_{k_i,sc,s,t}^{TES,Ch} \quad (8c)$$

$$0 \le H_{k_i,sc,s,t}^{TES,Dis} \le H^{TES,Dis,Max} I_{k_i,sc,s,t}^{TES,Dis} \quad (8d)$$

$$0 \le I_{k_i,sc,s,t}^{EES,Ch} + I_{k_i,sc,s,t}^{EES,Dis} \le 1 \quad (8e)$$

$$E_{k_i,sc,s,t=T}^{TES} = E_{k_i,sc,s,t=0}^{TES} \quad (8f)$$

$$E_{k_i,sc,s,t=0}^{TES} = \alpha_{k_i}^{initial} Cap^{Max,TES} \quad (8g)$$

$$H_{k_i,sc,s,t}^{TES,Ch} = H_{k_i,sc,s,t}^{CHP\to TES} + H_{k_i,sc,s,t}^{Boiler\to TES} + H_{k_i,sc,s,t}^{EH\to TES} + H_{k_i,sc,s,t}^{EHP\to TES} \quad (8h)$$

$$H_{k_i,sc,s,t}^{TES,Dis} = H_{k_i,sc,s,t}^{TES\to HL} + H_{k_i,sc,s,t}^{TES\to AC} \quad (8i)$$

- **RES model**

Eqs. (9a)-(9d) show the electrical power generation of the wind turbine and solar PV systems. The power balance equation of RESs is represented in (9d) [38].

$$P_{k_i,sc,s,t}^{PV} = \frac{G_{sc,s,t}^{a}}{G_0^{a}}\left[P_{k_i}^{PV,Max} + \mu_{P\max}\left(T_{sc,s,t}^{a} + G_{sc,s,t}^{a}\frac{NOCT-20}{800} - T_{M,0}\right)\right] \quad (9a)$$

$$P_{k_i,s,t}^{Wind} = \begin{cases} 0 & v_{sc,s,t}^{w} \le v_{ci} \\ p_{k_i}^{r}\left(\dfrac{v_{sc,s,t}^{w} - v_{ci}}{v_r - v_{ci}}\right)^3 & v_{ci} \le v_{sc,s,t}^{w} \le v_r \\ p_{k_i}^{r} & v_r \le v_{sc,s,t}^{w} \le v_{co} \\ 0 & v_{sc,s,t}^{w} \ge v_{co} \end{cases} \quad (9b)$$

$$P_{k_i,sc,s,t}^{RES} = P_{k_i,sc,s,t}^{PV} + P_{k_i,sc,s,t}^{Wind} \quad (9c)$$

$$P_{k_i,sc,s,t}^{RES} = P_{k_i,sc,s,t}^{RES\to EL} + P_{k_i,sc,s,t}^{RES\to EES} + P_{k_i,sc,s,t}^{RES\to EHP} + P_{k_i,sc,s,t}^{RES\to EH} + P_{k_i,sc,s,t}^{RES\to M} + P_{k_i,sc,s,t}^{RES\to G} + P_{k_i,sc,s,t}^{RES\to EVs} \quad (9d)$$

- **The coordinated power transaction constraints**

The electrical power transaction equation between the three residential, commercial, and industrial energy hubs are expressed in (10a)-(10r). As Eq. (10a) shows, the energy sold to the upstream grid by each hub is supplied by the CHP unit, EES system, EVs, and RESs. On the other hand, the power purchased from the upstream grid can be delivered to the EES system, EH, EHP, EVs, and electrical loads as indicated in (10b). Eqs. (10c)-(10d) specify the way that the energy sold to other hubs is supplied and how the energy purchased from other hubs is delivered to the assets. The power sold/purchased to/from other hubs is limited by constraints (10e) and (10f). Besides, the maximum electrical power trading between energy hubs is restricted by $P^{Trade,Max}$. Binary variables $I_{k_i,sc,s,t}^{H\to M}$ and $I_{k_i,sc,s,t}^{M\to H}$ relate to the electrical energy purchase and selling between the energy hubs. The electrical power purchased from the upstream grid is limited by (10g) and constraint (10h) limits the power sold to the upstream grid. It is noteworthy that as relationships (10i)-(10j) indicate, each hub can be either in the energy purchase or energy selling mode at each time. Constraints (10k) and (10l) state that the hub is not allowed to purchase energy from the upstream grid and sell it to other hubs, and vice versa. Assigning these constraints to the model would prevent the hubs from buying low-price energy and selling it to other hubs at higher prices.

$$P_{k_i,sc,s,t}^{H\to G} = P_{k_i,sc,s,t}^{CHP\to G} + P_{k_i,sc,s,t}^{EES\to G} + P_{k_i,sc,s,t}^{RES\to G} + P_{k_i,sc,s,t}^{EVs\to G} \quad (10a)$$

$$P_{k_i,sc,s,t}^{G\to H} = P_{k_i,sc,s,t}^{G\to EES} + P_{k_i,sc,s,t}^{G\to EH} + P_{k_i,sc,s,t}^{G\to EHP} + P_{k_i,sc,s,t}^{G\to EL} + P_{k_i,sc,s,t}^{G\to EVs} \quad (10b)$$

$$P_{k_i,sc,s,t}^{H\to M} = P_{k_i,sc,s,t}^{CHP\to M} + P_{k_i,sc,s,t}^{EES\to M} + P_{k_i,sc,s,t}^{RES\to M} + P_{k_i,sc,s,t}^{EVs\to M} \quad (10c)$$

$$P_{k_i,sc,s,t}^{M\to H} = P_{k_i,sc,s,t}^{M\to EES} + P_{k_i,sc,s,t}^{M\to EH} + P_{k_i,sc,s,t}^{M\to EHP} + P_{k_i,sc,s,t}^{M\to EL} + P_{k_i,sc,s,t}^{M\to EVs} \quad (10d)$$

$$0 \le P_{k_i,sc,s,t}^{H\to M} \le P^{Trade,Max} I_{k_i,sc,s,t}^{H\to M} \quad (10e)$$

$$0 \le P_{k_i,sc,s,t}^{M\to H} \le P^{Trade,Max} I_{k_i,sc,s,t}^{M\to H} \quad (10f)$$

$$0 \le P_{k_i,sc,s,t}^{G\to H} \le P^{Trans.,Max} I_{k_i,sc,s,t}^{G\to H} \quad (10g)$$

$$0 \le P_{k_i,sc,s,t}^{H\to G} \le P^{Trans.,Max} I_{k_i,sc,s,t}^{H\to G} \quad (10h)$$

$$0 \le I_{k_i,sc,s,t}^{M\to H} + I_{k_i,sc,s,t}^{H\to M} \le 1 \quad (10i)$$

$$0 \le I_{k_i,sc,s,t}^{G\to H} + I_{k_i,sc,s,t}^{H\to G} \le 1 \quad (10j)$$

$$0 \le I_{k_i,sc,s,t}^{G\to H} + I_{k_i,sc,s,t}^{H\to M} \le 1 \quad (10k)$$

$$0 \le I_{k_i,sc,s,t}^{M\to H} + I_{k_i,sc,s,t}^{H\to G} \le 1 \quad (10l)$$

The power transaction between the energy hubs is modeled as follows. Eqs. (10m)-(10o) determine the amount of power trading between one hub and other hubs. In addition, Eqs. (10p)-(10r) specify the amount of power received by each hub from the other two hubs.

$$P_{k_{Ind},sc,s,t}^{H\to M} = P_{sc,s,t}^{Ind\to Com} + P_{sc,s,t}^{Ind\to Res} \quad (10m)$$

$$P_{k_{Com},sc,s,t}^{H\to M} = P_{sc,s,t}^{Com\to Ind} + P_{sc,s,t}^{Com\to Res} \quad (10n)$$

$$P_{k_{Res},sc,s,t}^{H\to M} = P_{sc,s,t}^{Res\to Ind} + P_{sc,s,t}^{Res\to Com} \quad (10o)$$

$$P_{k_{Ind},sc,s,t}^{M\to H} = P_{sc,s,t}^{Res\to Ind} + P_{sc,s,t}^{Com\to Ind} \quad (10p)$$

$$P_{k_{Com},sc,s,t}^{M\to H} = P_{sc,s,t}^{Res\to Com} + P_{sc,s,t}^{Ind\to Com} \quad (10q)$$

$$P_{k_{Res},sc,s,t}^{M\to H} = P_{sc,s,t}^{Ind\to Res} + P_{sc,s,t}^{Com\to Res} \quad (10r)$$

- **Power balance constraints**

The electrical, heating and cooling power balance equations are represented in (11a)-(11c) respectively. These equations confirm are extracted from the nodal power injection method presented in [39]. As Eq. (11a) shows, the electrical power required by each hub is supplied by purchasing power from the upstream grid and other hubs, discharging power of the EES system and EVs, and the electrical power generated by the CHP unit and RESs. Moreover, it is possible that a fraction of the load demand, shown by $P_{k_i,sc,s,t}^{ENS}$ is not supplied. Eq. (11b) indicates that the CHP unit, EHP, EH, TES, and the boiler are supposed to supply the required heating power. The cooling power required by each hub is also supplied by the AC and EHP.

$$P_{k_i,sc,s,t}^{G\to EL} + P_{k_i,sc,s,t}^{M\to EL} + P_{k_i,sc,s,t}^{ESS\to EL} + P_{k_i,sc,s,t}^{EVs\to EL} + P_{k_i,sc,s,t}^{RES\to EL} + P_{k_i,sc,s,t}^{CHP\to EL} = P_{k_i,sc,s,t}^{EL} - P_{k_i,sc,s,t}^{ENS} \quad (11a)$$

$$H_{k_i,sc,s,t}^{CHP\to HL} + H_{k_i,sc,s,t}^{Boiler\to HL} + H_{k_i,sc,s,t}^{EHP\to HL} + H_{k_i,sc,s,t}^{EH\to HL} + H_{k_i,sc,s,t}^{TES\to HL} = H_{k_i,sc,s,t}^{HL} \quad (11b)$$

$$C_{k_i,sc,s,t}^{EHP\to CL} + C_{k_i,sc,s,t}^{AC\to CL} = C_{k_i,sc,s,t}^{CL} \quad (11c)$$

- **DRP model**

The DRP used in this study is modeled in (12a)-(12g). Eq. (12a) determines the load demand after applying the DRP, where $D_{k_i,sc,s,t}$ and $P^{EL}_{k_i,sc,s,t}$ are the load demand before and after applying the DRP at time *t* respectively. $D^{up}_{k_i,sc,s,t}$ and $D^{do}_{k_i,sc,s,t}$ show the amount of increase and decrease in the load demand as a result of applying the DRP. As Eq. (12b) states, the sum of the increases and the sum of decreases in the load demand should be equal. The increase or decrease in the load demand depends upon the load elasticity and hourly electricity price as modeled through (12c)-(12d). $\varepsilon^{up}_{k_i}$ and $\varepsilon^{do}_{k_i}$ denote increase and increase elasticities of the load demand respectively. $\lambda^{Buy}_{k_i,s,t}$ and $\lambda^{ref}_{k_i,s}$ are the electricity price at time *t* and over off-peak hours respectively. $B^{up}_{k_i}$ and $B^{do}_{k_i}$ are the coefficients of the maximum increase and decrease in the load demand due to applying the DRP as a percentage of the load demand respectively. It is noteworthy that $I^{up}_{k_i,sc,s,t}$ and $I^{do}_{k_i,sc,s,t}$ are binary variables, relating to the increase and decrease in the load demand respectively. Eq. (12g) states that the load demand increase and decrease cannot occur simultaneously at each time [38,40].

$$P^{EL}_{k_i,sc,s,t} = D_{k_i,sc,s,t} + D^{up}_{k_i,sc,s,t} - D^{do}_{k_i,sc,s,t} \tag{12a}$$

$$\sum_{t=1}^{T}\sum_{k_i\in K} D^{up}_{k_i,sc,s,t} = \sum_{t=1}^{T}\sum_{k_i\in K} D^{do}_{k_i,sc,s,t} \tag{12b}$$

$$D^{up}_{k_i,sc,s,t} \geq \varepsilon^{up}_{k_i} D_{k_i,sc,s,t}\left(1-\frac{\lambda^{Buy}_{k_i,s,t}}{\lambda^{ref}_{k_i,s}}\right) \tag{12c}$$

$$D^{do}_{k_i,sc,s,t} \geq \varepsilon^{do}_{k_i} D_{k_i,sc,s,t}\left(\frac{\lambda^{Buy}_{k_i,s,t}}{\lambda^{ref}_{k_i,s}}-1\right) \tag{12d}$$

$$0 \leq D^{up}_{k_i,sc,s,t} \leq D_{k_i,sc,s,t} B^{up}_{k_i} I^{up}_{k_i,sc,s,t} \tag{12e}$$

$$0 \leq D^{do}_{k_i,sc,s,t} \leq D_{k_i,sc,s,t} B^{do}_{k_i} I^{do}_{k_i,sc,s,t} \tag{12f}$$

$$0 \leq I^{up}_{k_i,sc,s,t} + I^{do}_{k_i,sc,s,t} \leq 1 \tag{12g}$$

- **EVs modeling**

The operation model of EVs has been presented in (13a)-(13i). The energy stored in the batteries of EVs is limited by constraint (13a). The hourly energy balance constraint of the battery is stated in (13b). Constraints (13c) and (13d) include the limitations of the charging and discharging power at each time interval *t*. Constraint (13e) removes the conflicting states in the charging and discharging modes at each time of the scheduling. It should be noted that charging/discharging is possible only in the parking lot. Accordingly, Eq. (13f) is valid only for the time the EV is in the parking. The amount of energy of EVs' batteries at the arrival and departure times are determined

using (13g) and (13h) respectively. The initial state-of-charge (SoC) of the EVs' batteries is randomly determined between 50% and 90%. Besides, in order to more motivate EV owners to participate in supplying the load demand, EVs not only receive the corresponding cost but also will have the SoC equal to the arrival time when they are departing the parking. The energy flow of the parking lot is indicated by (13i) and (13j). It is worth noting that T_a and T_d show the arrival time and departure time of EVs to/from the parking lot, respectively.

$$Cap^{Min,EV} \le E_{ev,sc,s,t}^{EV} \le Cap^{Max,EV} \tag{13a}$$

$$E_{ev,sc,s,t}^{EV} = E_{ev,sc,s,t-1}^{EV} + \left(P_{ev,sc,s,t}^{EV,Ch}\eta_{Ch}^{EV}\right)\Delta t - \left(\frac{P_{ev,sc,s,t}^{EV,Dis}}{\eta_{Dis}^{EV}}\right)\Delta t \tag{13b}$$

$$0 \le P_{ev,sc,s,t}^{EV,Ch} \le P^{EV,Ch,Max} I_{ev,sc,s,t}^{EV,Ch} \tag{13c}$$

$$0 \le P_{ev,sc,s,t}^{EV,Dis} \le P^{EV,Dis,Max} I_{ev,sc,s,t}^{EV,Dis} \tag{13d}$$

$$0 \le I_{ev,sc,s,t}^{EV,Ch} + I_{ev,sc,s,t}^{EV,Dis} \le 1 \quad , \quad T_a \le t \le T_d \tag{13e}$$

$$I_{ev,sc,s,t}^{EV,Ch} + I_{ev,sc,s,t}^{EV,Dis} = 0 \quad , \quad t \le T_a \text{ or } t \ge T_d \tag{13f}$$

$$E_{ev,sc,s,t=T_a}^{EV} = \alpha_{ev}^{Initial} Cap^{Max,EV} \tag{13g}$$

$$E_{ev,sc,s,t=T_d}^{EV} = E_{ev,sc,s,t=T_a}^{EV} \tag{13h}$$

$$\sum_{ev_{k_i}=1}^{EV_{k_i}} P_{ev,sc,s,t}^{EV,Ch} = P_{k_i,sc,s,t}^{G\to EVs} + P_{k_i,sc,s,t}^{CHP\to EVs} + P_{k_i,sc,s,t}^{RES\to EVs} + P_{k_i,sc,s,t}^{M\to EVs} \tag{13i}$$

$$\sum_{ev_{k_i}=1}^{EV_{k_i}} P_{k_i,sc,s,t}^{EV,Dis} = P_{k_i,sc,s,t}^{EVs\to EL} + P_{k_i,sc,s,t}^{EVs\to G} + P_{k_i,sc,s,t}^{EVs\to EHP} + P_{k_i,sc,s,t}^{EVs\to EH} + P_{k_i,sc,s,t}^{EVs\to M} \tag{13j}$$

- **ACOPF constraints**

The ACOPF constraints are stated in equations (14a)-(14l). The susceptance and conductance values are calculated as (14a). The active power and reactive power flows of feeders are shown in Eqs. (14b) and (14c), respectively. It is noteworthy that the load demand at the point of hub connection is determined with respect to the amount of energy purchased from the grid and other hubs as stated in (14d). Eq. (14e) specifies the reactive power demand of each hub with regard to the active power purchased, and taking into account the distribution system standards [41]. The bus at which the energy hub is connected would be a PV bus over the hours it delivers power to the upstream grid and other hubs as stated in (14f). As (14g) emphasizes, the reactive power of the energy hub with respect to its generative nature in this state should be within the permitted range. The active and reactive power balance equations at each bus are expressed in Eqs. (14h) and (14i) respectively, with respect to the amount of power generation, load demand, and transacted power [42]. Furthermore, bus 1 has been assigned to the model as the slack bus, taking into account the

radial configuration of the system. The constraints of the bus voltage and line flow are represented in Eqs. (14k) and (14l), respectively [43].

$$G_l = \frac{r_l}{r_l^2 + x_l^2}, \quad B_l = \frac{x_l}{r_l^2 + x_l^2} \tag{14a}$$

$$P_{l,sc,s,t}^{flow} = G_l \left[V_{n,sc,s,t}^2 - V_{n,sc,s,t} V_{m,sc,s,t} \cos(\delta_{n,sc,s,t} - \delta_{m,sc,s,t}) \right] + B_l V_{n,sc,s,t} V_{m,sc,s,t} \sin(\delta_{n,sc,s,t} - \delta_{m,sc,s,t}) \quad , \quad \forall l : n \to m \tag{14b}$$

$$Q_{l,sc,s,t}^{flow} = B_l \left[V_{n,sc,s,t}^2 - V_{n,sc,s,t} V_{m,sc,s,t} \cos(\delta_{n,sc,s,t} - \delta_{m,sc,s,t}) \right] - G_l V_{n,sc,s,t} V_{m,sc,s,t} \sin(\delta_{n,sc,s,t} - \delta_{m,sc,s,t}) \quad , \quad \forall l : n \to m \tag{14c}$$

$$P_{n,sc,s,t}^{Demand} = \sum_{k_i \in n} P_{k_i,sc,s,t}^{G \to H} + P_{k_i,sc,s,t}^{M \to H} \tag{14d}$$

$$Q_{n,sc,s,t}^{Demand} = \sum_{k_i \in n} \tan(\varphi_{k_i}) \left(P_{k_i,sc,s,t}^{G \to H} + P_{k_i,sc,s,t}^{M \to H} \right) \tag{14e}$$

$$P_{n,sc,s,t}^{Gen} = \sum_{k_i \in n} P_{k_i,sc,s,t}^{H \to G} + P_{k_i,sc,s,t}^{H \to M} \tag{14f}$$

$$-\sum_{k_i \in n} \alpha_{k_i}^{fed} \left(P_{k_i,sc,s,t}^{H \to G} + P_{k_i,sc,s,t}^{H \to M} \right) \le Q_{n,sc,s,t}^{Gen} \le \sum_{k_i \in n} \alpha_{k_i}^{inject} \left(P_{k_i,sc,s,t}^{H \to G} + P_{k_i,sc,s,t}^{H \to M} \right) \tag{14g}$$

$$P_{n,sc,s,t}^{Gen} + \sum_{l=1|m \to n}^{L} P_{l,sc,s,t}^{flow} = P_{n,sc,s,t}^{Demand} + \sum_{l=1|n \to m}^{L} P_{l,sc,s,t}^{flow} \tag{14h}$$

$$Q_{n,sc,s,t}^{Gen} + \sum_{l=1|m \to n}^{L} Q_{l,sc,s,t}^{flow} = Q_{n,sc,s,t}^{Demand} + \sum_{l=1|n \to m}^{L} Q_{l,sc,s,t}^{flow} \tag{14i}$$

$$P_{1,sc,s,t}^{Gen} = P_{sc,s,t}^{Sub} \tag{14j}$$

$$V_n^{\min} \le V_{n,sc,s,t} \le V_n^{\max} \tag{14k}$$

$$-S_l^{\max} \le \sqrt{(P_{l,sc,s,t}^{flow})^2 + (Q_{l,sc,s,t}^{flow})^2} \le S_l^{\max} \tag{14l}$$

4- Methodology

Fig. 3 illustrates the flowchart of the model proposed in this paper. The upper level solves the coordinated/uncoordinated operation problem of energy hubs using the CPLEX solver in the GAMS software. Afterward, the data, including the power transactions between hubs and the power transactions between hubs and the upstream grid are sent to MATLAB/MATPOWER for the ACOPF calculations. If all ACOPF constraints are satisfied, the solution converges and the process finishes. Otherwise, the violation from the ACOPF constraint is reported to the first stage and the problem is solved with the updated data. These iterations continue until the solution converges.

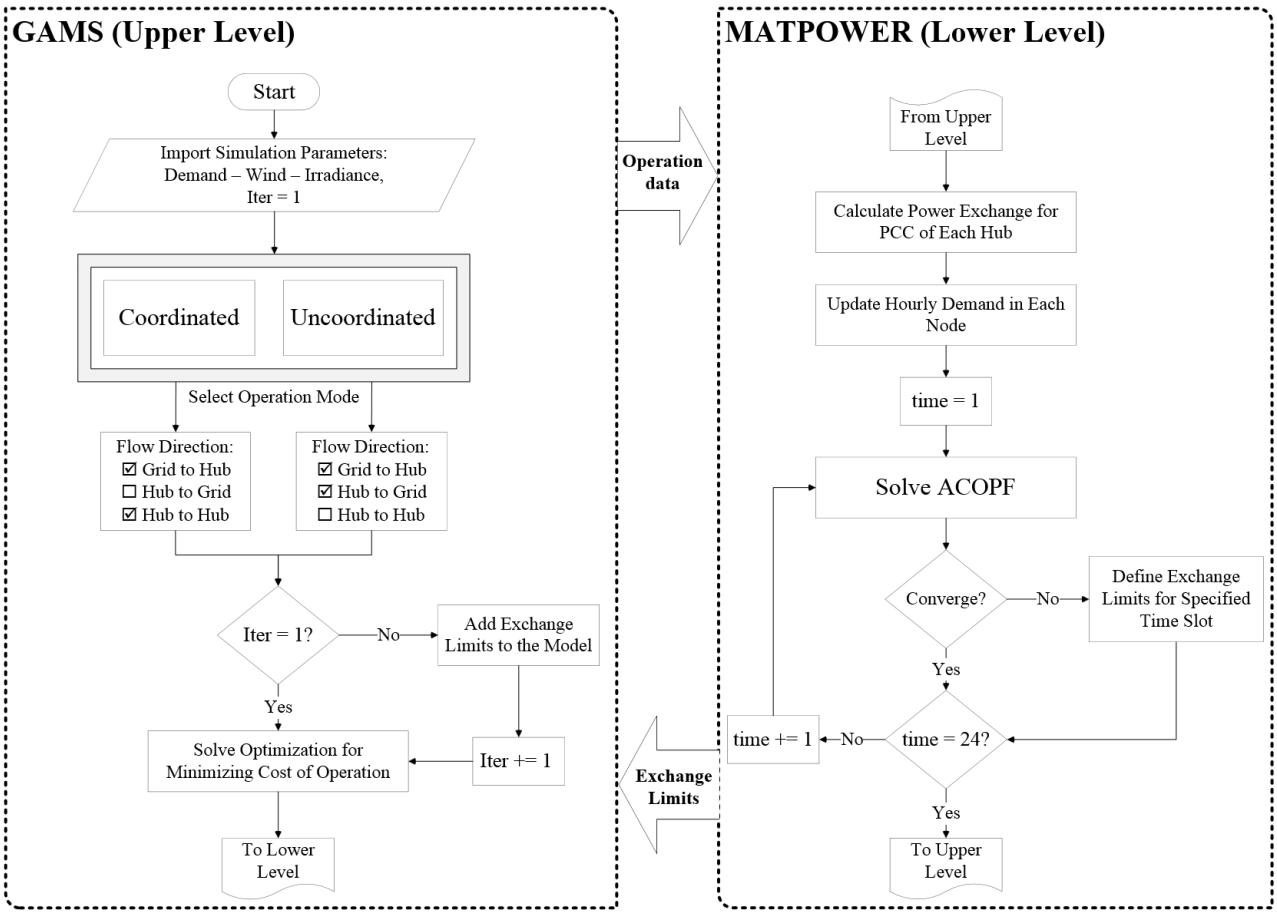

Fig. 3. The flowchart of the proposed model.

5- Simulation results

The proposed energy hub management problem has been modeled in a MILP framework. The data of the hubs' assets are shown in Fig. 1. Besides, the data of the system is in accordance with the IEEE 33-bus distribution system [44].

Table 1. The technical data of energy hub assets [37,45].

CHP		**Emission parameters**	
η_P^{CHP}	*55 %*	$EF_{em}^{CHP\ CO2}$	*1.596*
η_H^{CHP}	*45 %*	$EF_{em}^{CHP\ SO2}$	*0.008*
Boiler		$EF_{em}^{CHP\ NO2}$	*0.44*
η^{Boiler}	*85*	$EF_{em}^{B\ CO2}$	*1.755*
EES / TES / EV		$EF_{em}^{B\ SO2}$	*1.011*
$\eta_{CH}^{EES/TES}$	*90 %*	$EF_{em}^{B\ NO2}$	*0.62*
$\eta_{Dis}^{EES/TES}$	*90 %*	$EF_{em}^{G\ CO2}$	*1.432*
λ^{EES}	*0.02 $*	$EF_{em}^{G\ SO2}$	*0.454*
λ^{TES}	*0.02 $*	$EF_{em}^{G\ NO2}$	*2.1*
λ^{EV}	*0.06 $*	λ_{em}^{CO2}	*0.00014 $*

Electrical heater		λ_{em}^{SO2}	*0.0099 $*		
η^{EH}	*85 %*	λ_{em}^{NO2}	*0/042 $*		
Absorption chiller		**The capacities of hub equipment**			
η^{AC}	*85 %*				
Transformer and Converter		***asset***	***Ind.***	***Com.***	***Res.***
$\eta_{ee}^{T/Con}$	*0.9*	$Cap^{max,CHP}$	*5000*	*900*	*1500*
EHP		$P^{max,CHP}$	*3000*	*500*	*800*
η_{C}^{EHP}	*85 %*	$H^{max,CHP}$	*2000*	*400*	*700*
η_{H}^{EHP}	*85%*	$Cap^{max,Boiler}$	*800*	*200*	*300*
DRP		$Cap^{max,EHP}$	*600*	*300*	*300*
$D_{k_i,sc,s,t}^{up}$	*0.04*	$Cap^{max,AC}$	*1000*	*200*	*400*
$D_{k_i,sc,s,t}^{do}$	*0.03*	$Cap^{max,EH}$	*300*	*100*	*100*
$B_{k_i}^{up}$	*0.05*	$Cap^{max,EES}$	*600*	*300*	*300*
$B_{k_i}^{up}$	*0.05*	$Cap^{max,TES}$	*400*	*100*	*200*
$\lambda_{k_i,s}^{Ref}$	$mean(\lambda_{k_i,s,}^{buy})$	*RES*	*400*	*100*	*100*

Table 2 represents the price of the energy purchased from the grid for each hub. Table 3 includes the seasonal load demand of each hub. In this respect, the proposed problem has been solved both in the coordinated and uncoordinated operation modes to assess their impacts on the operating cost and the load demand-supply under contingent events. As has been previously mentioned, any energy hub can transact power with other hubs, but the purchase and selling prices would be different due to the different applications of the hubs.

Table 2. Electricity price (Cent/kWh)

Hour	**Industrial**			**Commercial**			**Residential**		
	Spr./Fall	Summer	Winter	Spr./Fall	Summer	Winter	Spr./Fall	Summer	Winter
1	9.72	11.88	9.234	4.8	6	4.32	6.48	6.48	6.16
2	9.72	11.88	9.234	4.8	6	4.32	6.48	6.48	6.16
3	9.72	11.88	9.234	4.8	6	4.32	6.48	6.48	6.16
4	9.72	11.88	9.234	4.8	6	4.32	6.48	6.48	6.16
5	9.72	11.88	9.234	4.8	6	4.32	6.48	6.48	6.16
6	9.72	11.88	9.234	4.8	6	4.32	6.48	6.48	6.16
7	9.72	11.88	9.234	4.8	6	4.32	9	10.8	6.16
8	28.8	36	27.36	4.8	6	4.32	9	10.8	9.23
9	28.8	36	27.36	4.8	6	12.72	9	10.8	9.23
10	28.8	36	27.36	14.4	18	12.72	9	10.8	9.23
11	28.8	36	27.36	14.4	18	12.72	12.6	18	9.23
12	28.8	36	27.36	14.4	18	12.72	12.6	18	9.23
13	28.8	36	27.36	14.4	18	12.72	12.6	18	9.23
14	28.8	36	27.36	14.4	18	12.72	12.6	18	9.23
15	28.8	36	27.36	14.4	18	12.72	12.6	18	9.23
16	28.8	36	27.36	14.4	18	12.72	12.6	18	9.23
17	28.8	36	27.36	14.4	18	12.72	12.6	18	11.97
18	9.72	36	9.234	16.8	18	12.72	12.6	18	11.97
19	9.72	11.88	9.234	16.8	24	12.72	12.6	10.8	11.97
20	9.72	11.88	9.234	16.8	24	12.72	12.6	10.8	11.97

21	9.72	11.88	9.234	16.8	24	10.8	12.6	10.8	11.97
22	9.72	11.88	9.234	14.4	24	10.8	9	10.8	6.16
23	9.72	11.88	9.234	14.4	24	10.8	6.48	6.48	6.16
24	9.72	11.88	9.234	4.8	6	4.32	6.48	6.48	6.16

Table 3. Electrical load demand (kW)

Hour	Industrial			Commercial			Residential		
	Spr./Fall	Summer	Winter	Spr./Fall	Summer	Winter	Spr./Fall	Summer	Winter
1	1200	1200	800	175	175	175	401.5	584.5	190.4
2	1200	1200	800	175	175	175	400.4	551.9	259.6
3	1200	1200	800	175	175	175	384.9	520.0	273.4
4	1200	1200	800	175	175	175	380.9	499.6	304.3
5	1600	1600	2000	175	175	175	448.7	576.2	386.4
6	2400	2000	2800	175	175	175	587.1	733.5	551.5
7	3200	2800	3600	175	175	175	780.0	893.5	638.6
8	3800	3600	4000	175	175	175	855.1	910.0	730.8
9	4000	4000	4000	280	280	280	899.5	910.0	729.0
10	4000	4000	4000	420	420	420	913.8	910.0	732.2
11	4000	4000	4000	490	490	490	911.7	975.0	780.0
12	4000	4000	4000	490	490	490	931.5	1105.0	780.0
13	4000	4000	4000	490	490	490	947.1	1105.0	780.0
14	4000	4000	4000	490	490	490	962.9	975.0	780.0
15	4000	4000	4000	542.5	525	560	976.7	845.0	845.0
16	4000	4000	3600	542.5	525	560	980.4	845.0	845.0
17	2800	3600	3200	577.5	560	595	985.9	910.0	780.0
18	2400	2800	2000	595	560	630	1020.6	975.0	715.0
19	1600	1600	800	665	630	700	1019.2	1040.0	715.0
20	1200	1200	800	700	700	700	979.2	1170.0	715.0
21	1200	1200	800	700	700	700	878.0	1300.0	624.0
22	1200	1200	800	647.5	700	595	730.0	1248.0	596.0
23	1200	1200	800	595	700	490	581.4	1040.0	397.2
24	1200	1200	800	385	490	280	414.0	780.0	192.6

5-1- Case study 1

The problem of energy hub management is solved in this section both for the coordinated and uncoordinated operation modes. It is worth noting that in the coordinated operation mode, hubs are allowed to trade energy with each other and the upstream grid, while they are not permitted to sell energy to the upstream grid. In the uncoordinated operation mode, the power transaction between the energy hubs is not allowed and each hub would be permitted to transact power with the upstream grid. Table 4 represents the annual operating cost for both operation modes. This table shows, the operating cost has reduced using the coordinated operation. It is due to the possibility of power transaction of the hubs with each other.

Table 4. The annual costs of coordinated and uncoordinated operation modes: Case 1.

Type of Energy Hubs	Operating Mode					
	Coordinated			Uncoordinated		
	OC ($)	Buy ($)	Sell ($)	OC ($)	Buy ($)	Sell ($)
Industrial	4064159.20	601371.42	86118.88	4116821.11	589395.54	14516.90
Commercial	378339.38	77628.48	34798.57	401243.79	60092.05	9870.77
Residential	497886.09	119091.65	3272.05	553761.95	114552.91	351.84
Convergence Time (sec)		2.496			2.506	

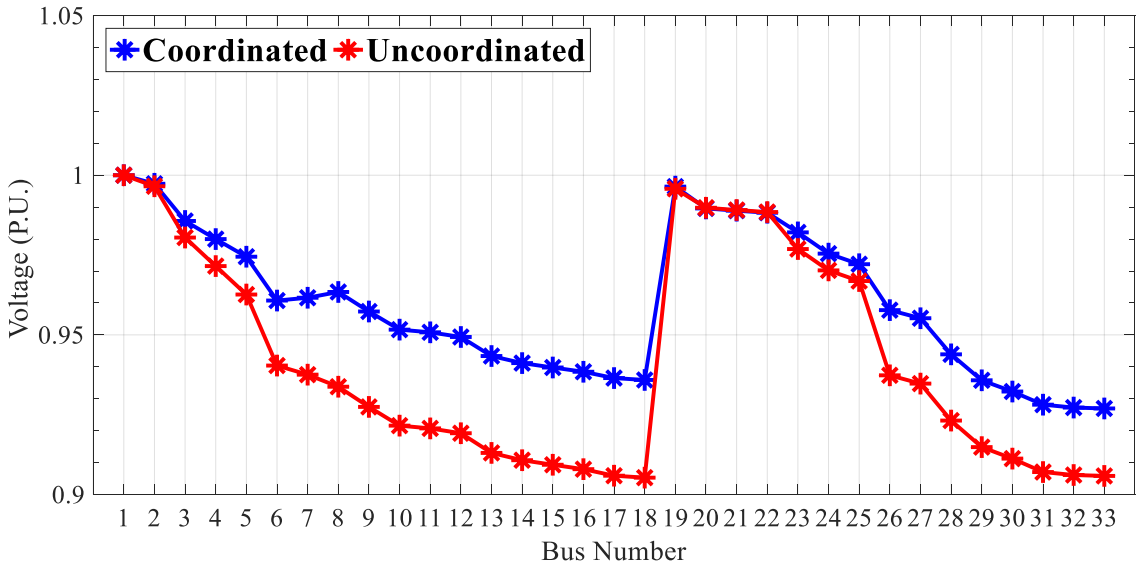

(a)

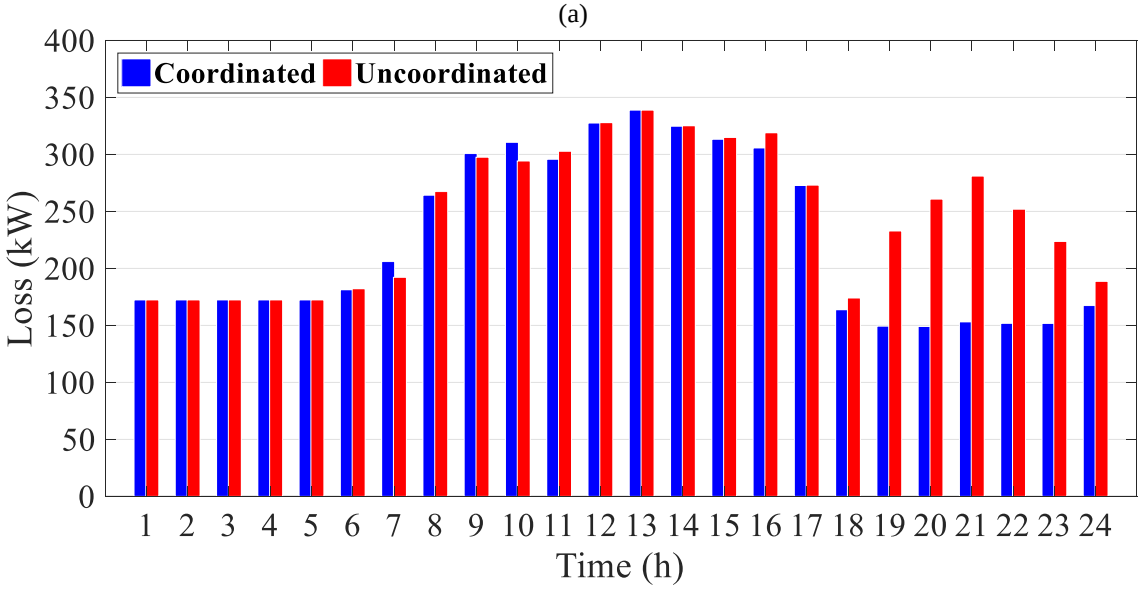

(b)

Fig. 4. (a) The voltage of each bus at 20:00 h in summer; (b) The hourly power losses in the coordinated and uncoordinated operation modes.

Besides, the energy purchase cost in the coordinated mode has substantially increased compared to the case with the uncoordinated operation. On the other hand, the profit made by selling energy has significantly increased for all hubs. It is due to the fact that each hub prefers to supply its power shortage by transacting power with other hubs rather than purchasing power from the upstream grid. In this situation, the energy hub would not be supposed to pay any cost due to emissions. Moreover, the magnitude of the voltage at hour 20 is provided in Fig. 4 (a) and the hourly power losses have been calculated for the two operation modes and the results obtained are shown in Fig. 4(b). This figure verifies that the losses have reduced using the coordinated operation mode. The substantial difference between the final hours and the middle of the day is due to the fact that the residential and commercial hubs purchase their required power from the industrial hub instead of the upstream grid. It is noteworthy that the load demand of the industrial hub is relatively low over these hours and its generation capacity can be employed to supply the load demand of the other two hubs.

5-1-1- The scheduling results of case 1

Figs. 5-7 depict the electrical power transaction between the three energy hubs in the coordinated operation mode. The results obtained from simulating the coordinated operation model show that the industrial hub sells energy to the residential and commercial energy hubs between hours 17 to 24 in all seasons. It is noted that the load demand of the industrial hub is low over these non-working hours and this energy hub can make a profit by selling energy. As can be observed, the amount of power sold to the residential and commercial hubs is considerably higher as the load demand of these two hubs is significantly higher in summer.

Figs. 6(a) and 6(b) show the seasonal amount of power sold to the industrial and residential hubs by the commercial hub. As can be seen, the commercial hub sells energy to the industrial hub over the initial hours of the day in all seasons. By approaching the middle of the day, this amount reduces due to the higher load demand of the commercial hub and lower available energy. As Fig. 6(d) illustrates, the amount of energy sold to the residential hub is much lower and it occurs only in spring and summer.

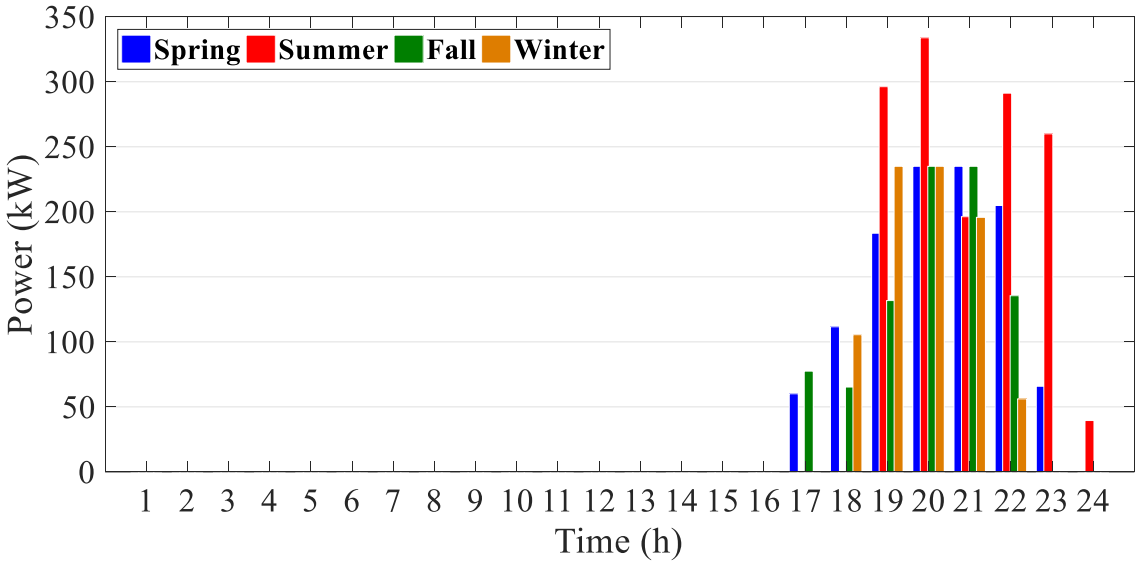

(a)

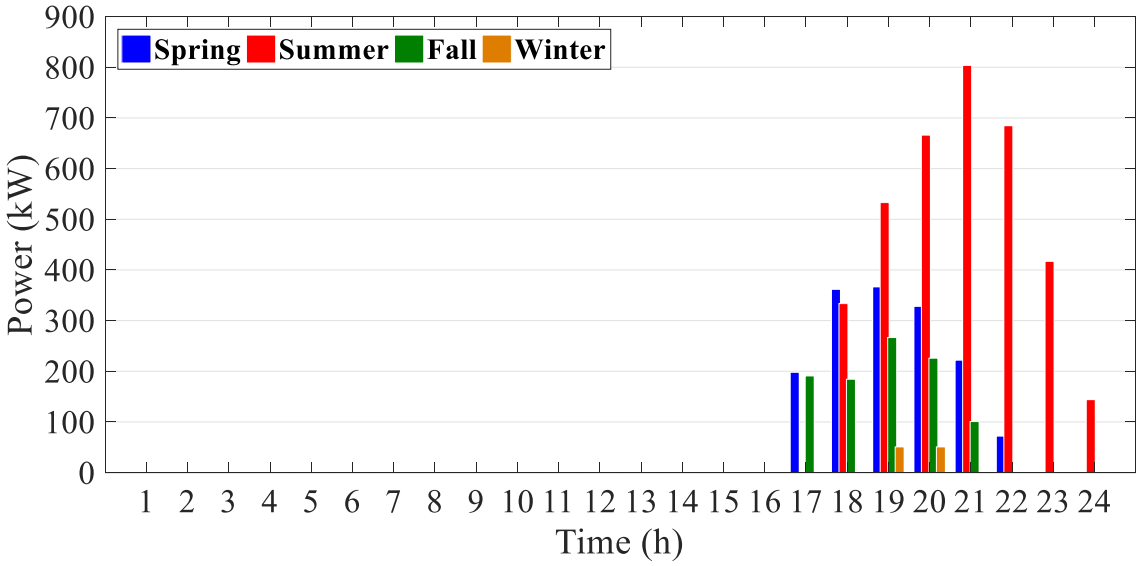

(b)

Fig. 5. (a) Industrial hub to commercial hub; (b) Industrial hub to residential hub.

The amount of power sold to the industrial and commercial hubs by the residential hub is shown in Figs 7(a) and 7(b). As can be observed in these figures, no energy has been sold in summer by the residential hub due to its high load demand over this period. Similar to the commercial hub, the amount of energy sold by the residential hub reduces while approaching the middle of the day due to its higher load demand during these hours. Fig. 7(b) depicts that the power sold to the

commercial hub by the residential hub is over the final hours of the day and only in fall and winter. It is due to the fact that the load demand of the residential hub is almost zero during these intervals and it can make a profit by selling power.

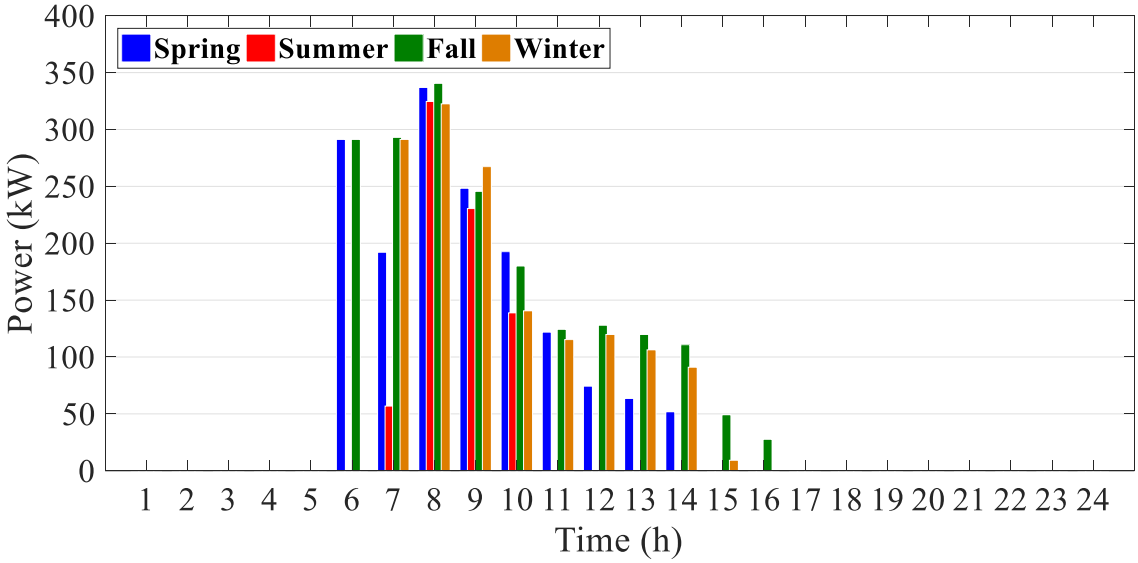

(a)

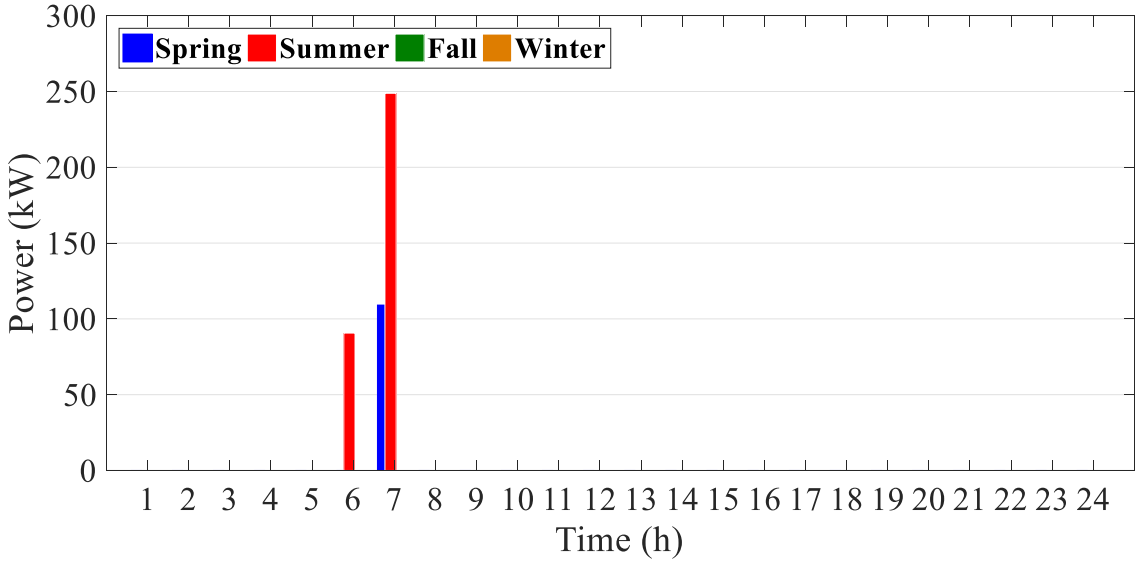

(b)

Fig. 6. (a) Commercial hub to industrial hub; (b) Commercial hub to residential hub

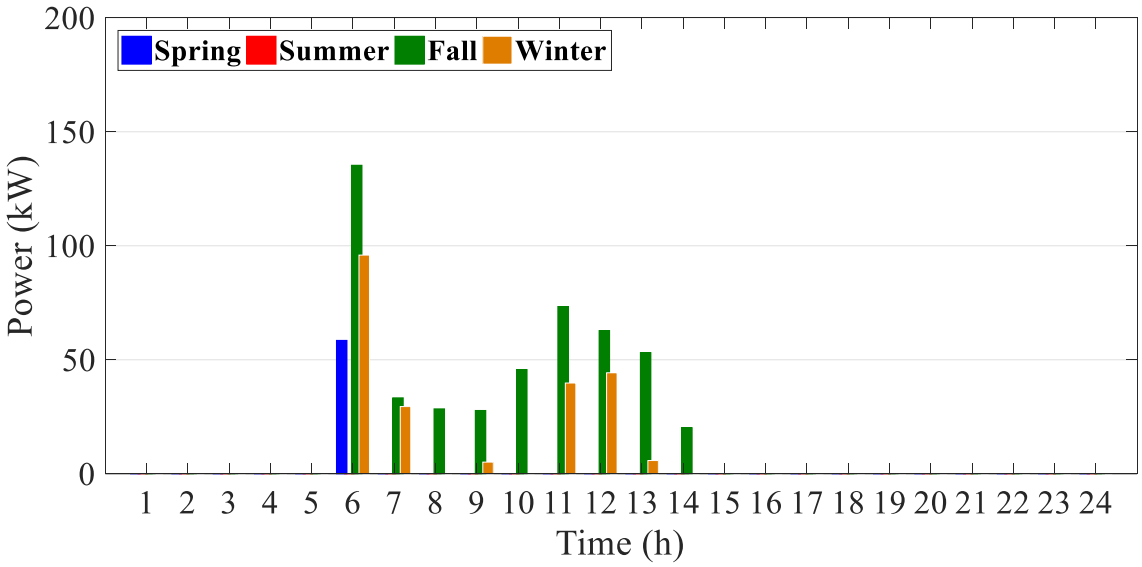

(a)

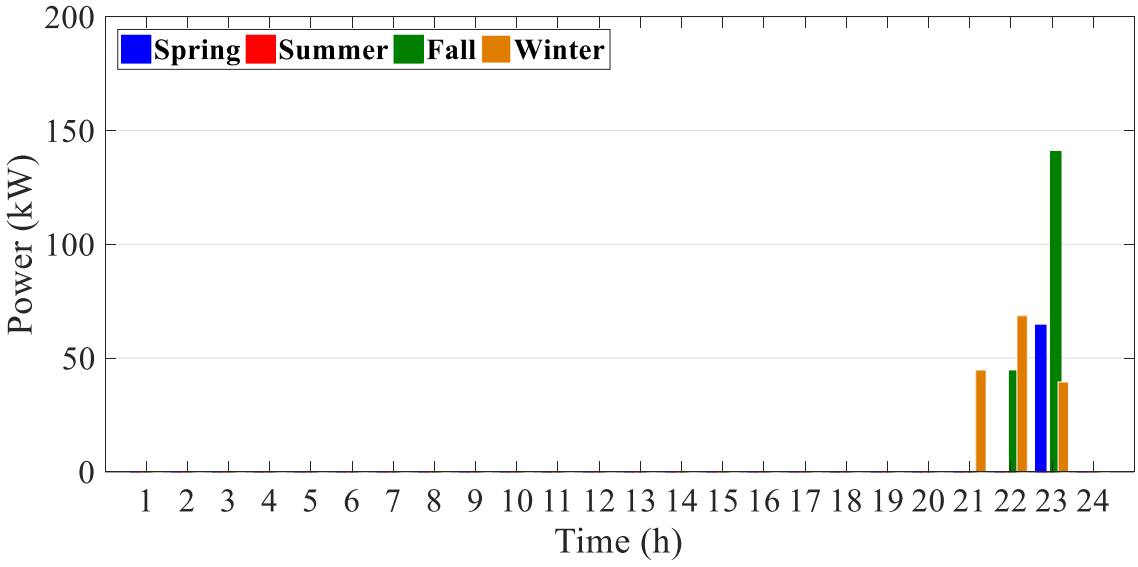

(b)

Fig. 7. (a) Residential to industrial; (b) Residential to commercial

It has been mentioned above that each hub can supply its power shortage both by transacting power with other hubs and the upstream grid in the coordinated operation mode. On the other hand, by using the uncoordinated operation model, an energy hub cannot trade energy with other hubs. Consequently, the only solution to their power shortage would be to transact power with the upstream grid.

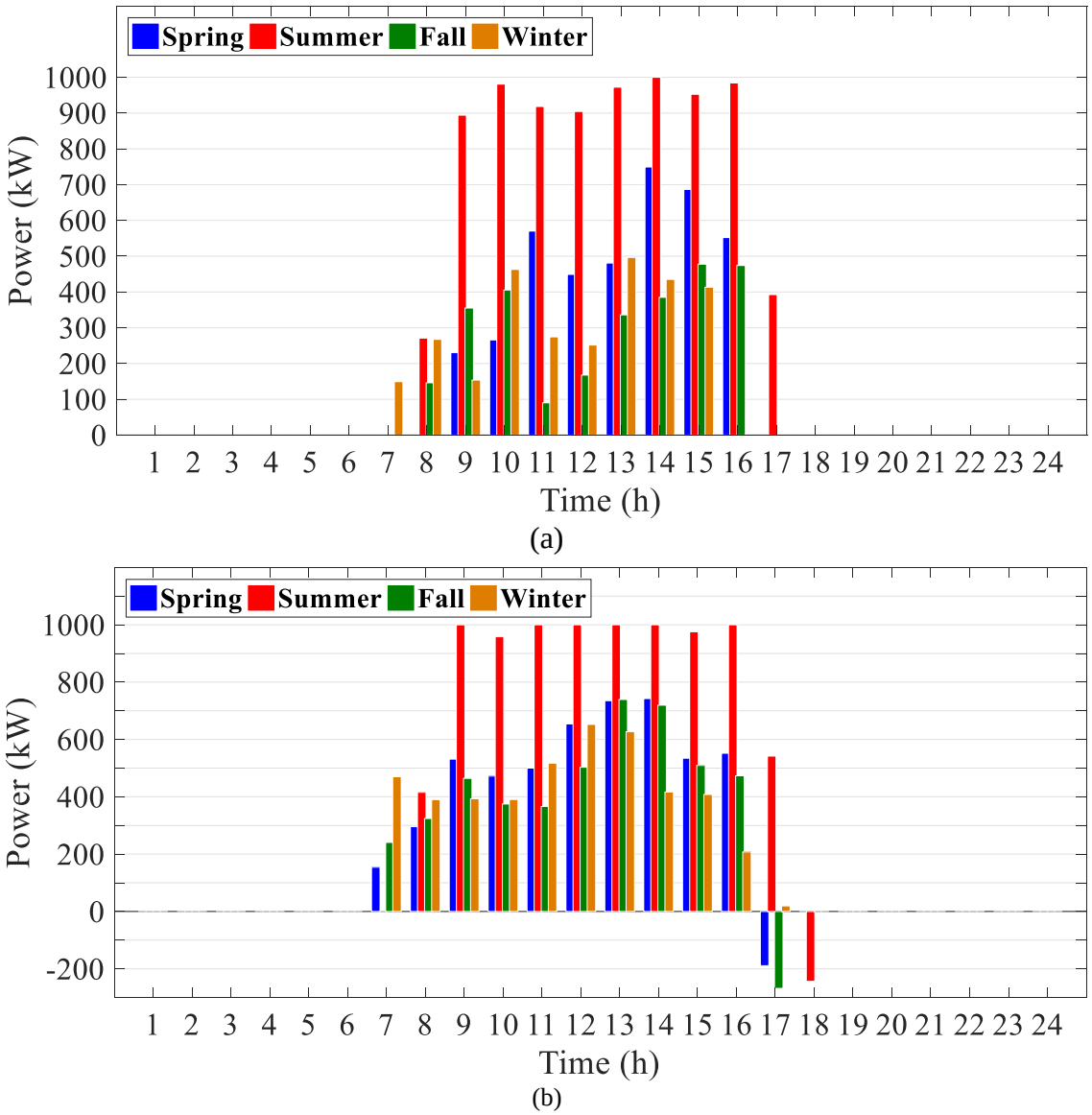

Fig. 8. Industrial hub's power transaction with the grid in the coordinated mode; (b) Industrial hub' power transaction with the grid in the uncoordinated mode.

In this respect, Figs. 8-10 depict the amount of power purchased from the upstream grid by each energy hub in the coordinated and uncoordinated operation modes. As it is expected, the results show a substantial increase in the amount of power purchased from the upstream grid. It is due to the impossibility of the energy trading between the energy hubs in the uncoordinated operation mode.

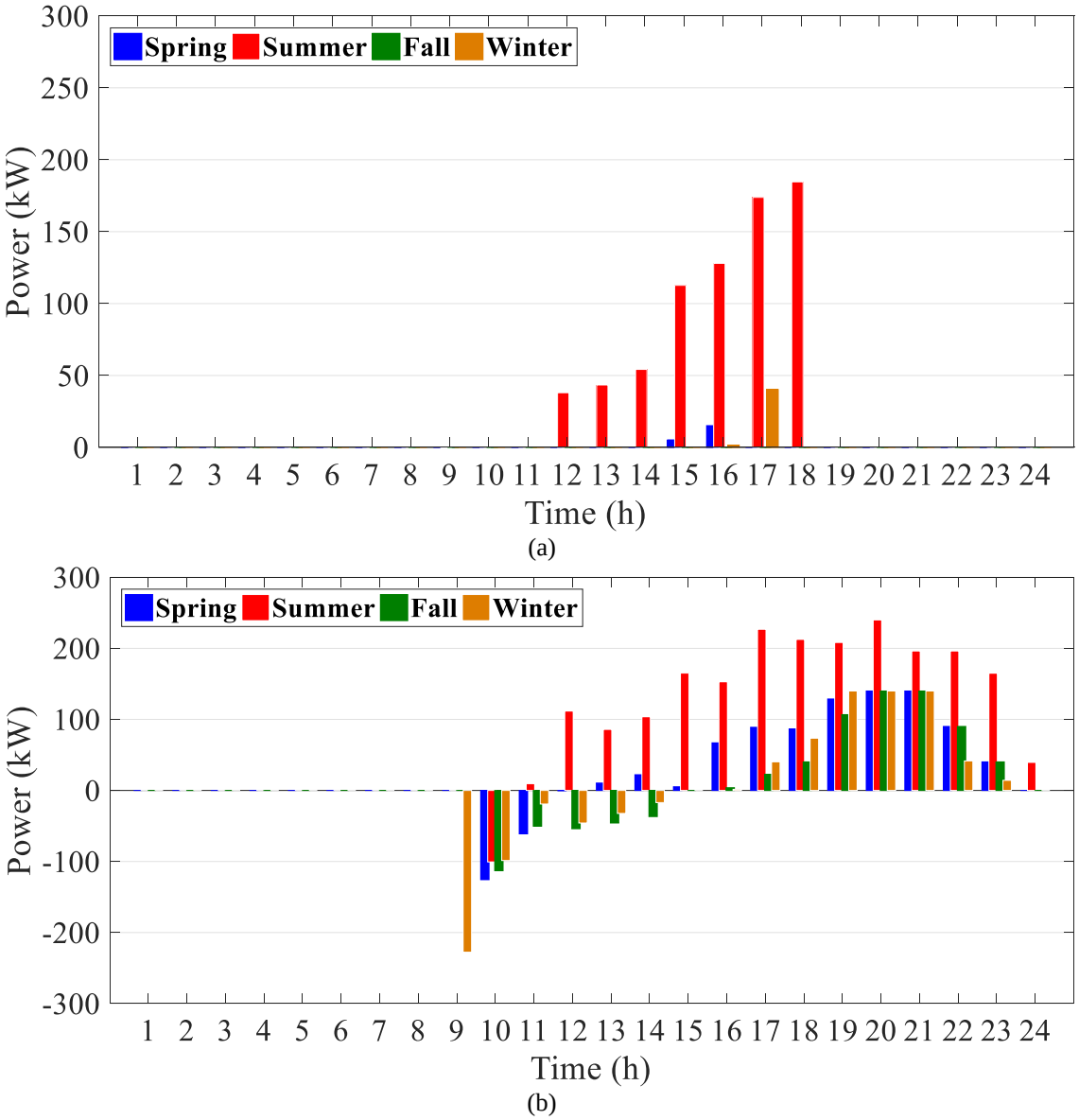

Fig. 9. (a) Commercial hub's power transaction with the grid in the coordinated mode; (b) Commercial hub's power transaction with the grid in the uncoordinated mode.

Table 5. Operating costs without and with the DRP.

Mode	Without the DRP				With the DRP			
Season	**Winter**	**Spring**	**Summer**	**Fall**	**Winter**	**Spring**	**Summer**	**Fall**
Industrial	9995.9	10560.5	20773.9	11118.4	9581.6	10195.0	13963.2	10798.9
Commercial	809.9	1020.0	1437.8	930.1	803.5	1007.4	1411.5	923.7
Residential	864.2	1310.7	2478.8	1013.5	844.2	1253.1	2365.6	993.4

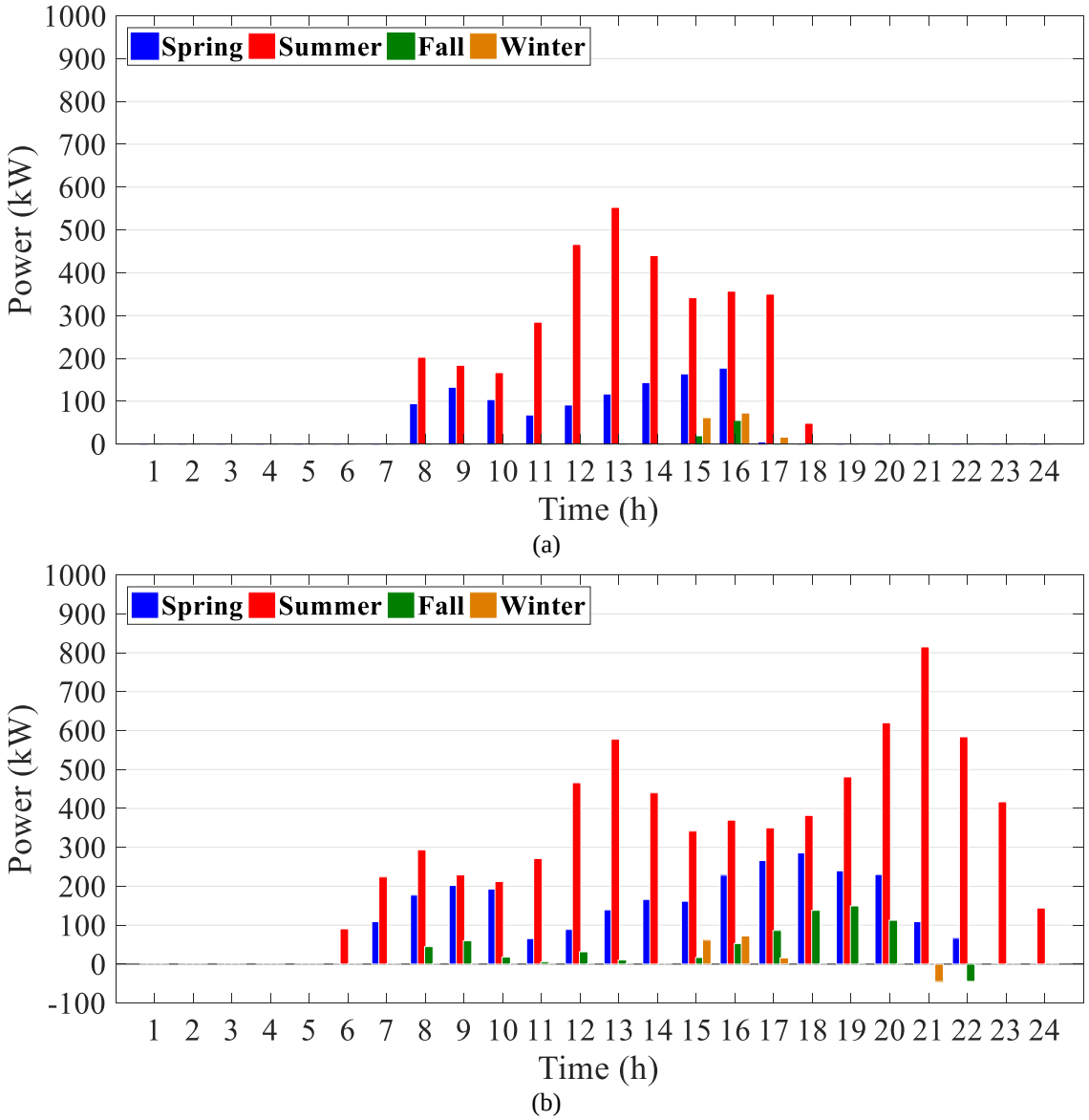

Fig. 10. (a) Residential hub's power transaction with the grid in the coordinated mode; (b) Residential hub's power transaction with the grid in the uncoordinated mode.

Fig. 11 shows the operation results of the parking lot located in the industrial hub for the coordinated and uncoordinated operation modes. As can be observed from this figure, EVs inject power to the parking lot over the initial hours and middle of the day to contribute to supplying the load demand and they charge over the final hours of the day.

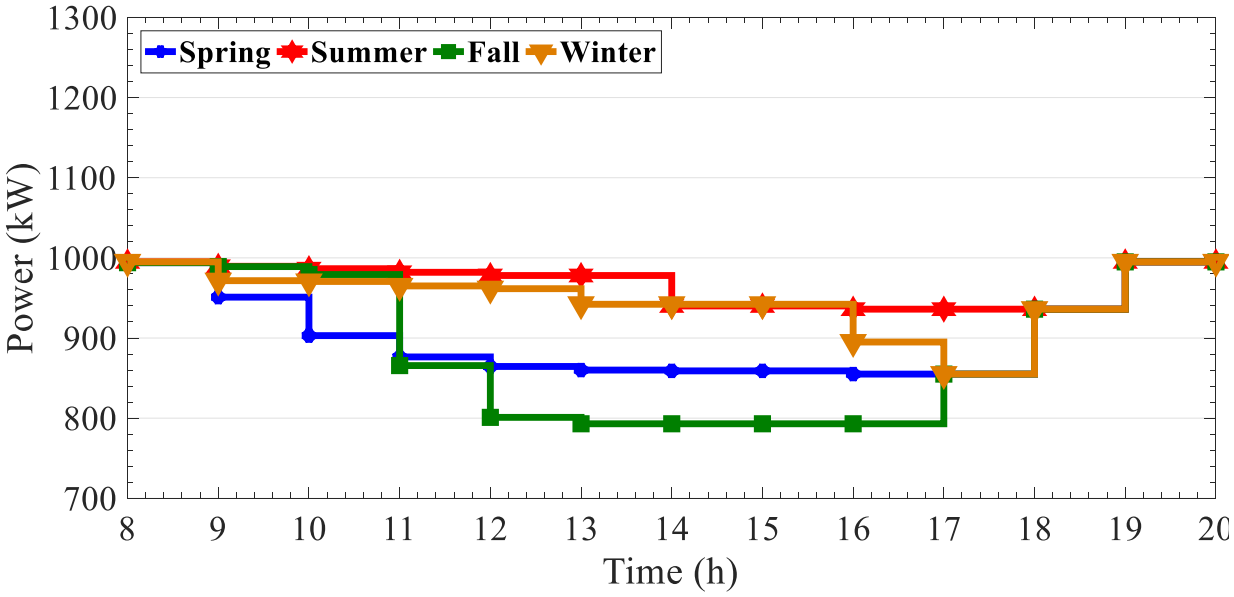

(a)

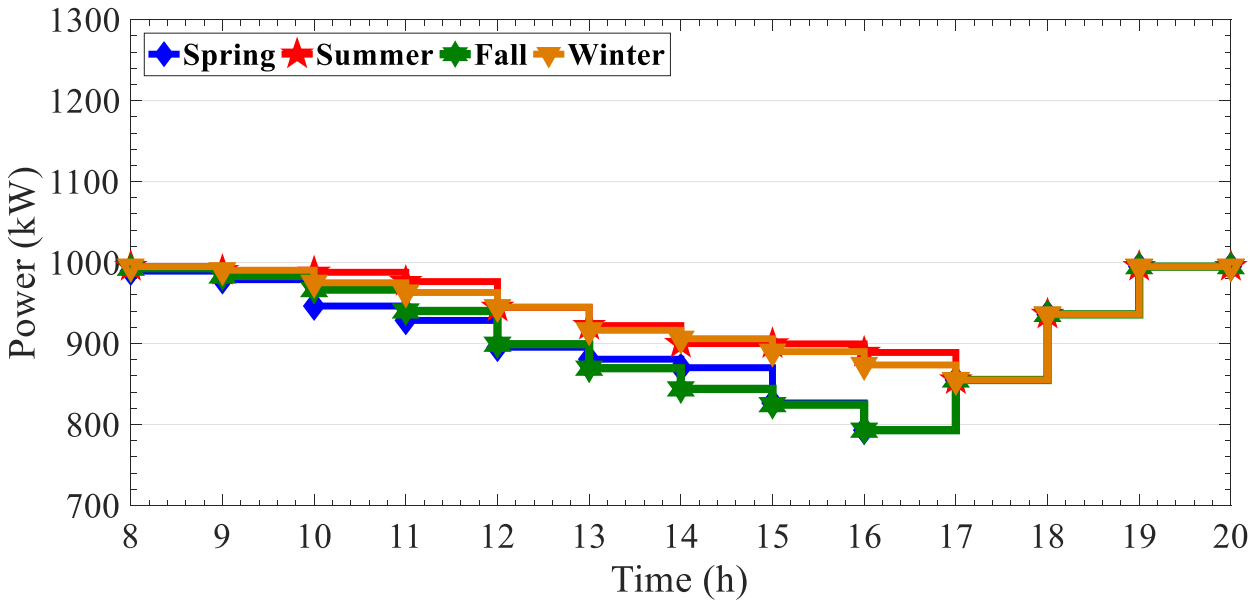

(b)

Fig. 11. (a) SoC of EVs in the coordinated operation mode; (b) SoC of EVs in the uncoordinated operation mode.

This paper utilized a price-based DRP to alleviate the operating cost. In this respect, Table 5 represents the operating cost of each hub with and without the DRP in each season. The results

show a considerable reduction in the operating cost in case the DRP is applied. Table 6 includes the seasonal emission costs of each hub for the coordinated and uncoordinated operation modes. As this table shows, the emission costs are higher in the uncoordinated operation mode. It is due to the higher energy purchased from the upstream grid in the uncoordinated mode.

Table 6. The seasonal emission costs for the coordinated and uncoordinated operation modes.

	Operating Mode							
Type of Energy Hubs	Coordinated				Uncoordinated			
	TEC	CO2	NO2	SO2	TEC	CO2	NO2	SO2
Industrial	632672.73	5705.24	617574.43	9393.06	662811.04	5628.27	645687.75	11495.02
Commercial	104602	1108.81	102756.25	736.94	126000.03	1090.57	122842.54	2066.92
Residential	143584.62	1321.39	139903.86	2359.36	195257.78	1421.93	188926.55	4909.30

5-2- Case study 2

In this case study, in order to investigate the effect of uncertainties on scheduling results, the problem has been solved by considering the uncertainties of electrical, cooling and heating loads, the output power of RESs and EV drivers' behavior. It should be mentioned that initially 1000 scenarios were generated for each uncertain parameter. In this regard, loads and EVs scenarios are generated by the beta distribution function, while wind speed and solar radiation scenarios are generated by the Weibull and beta distribution functions, respectively. Then, in order to reduce the computational burden, the number of initial scenarios is reduced to 10 by the k-means clustering algorithm. Figs. 12-14 indicate the scenarios obtained for different loads in residential, industrial and commercial hubs. As can be seen, the demand curves are different in each season. Moreover, Fig. 15 presents the obtained scenarios for solar radiation, wind speed and EVs.

Table 7 presents the scheduling results obtained from Case 2. It should be noted that the results are presented as expected values. As the table shows, operating costs in both coordinate and uncoordinated modes have increased compared to deterministic conditions, due to uncertainties. Numerical results demonstrate that the operating costs in the coordinated mode in industrial, residential and commercial hubs have increased by 7.06%, 9.85% and 10.24%, respectively, compared to case 1 (deterministic conditions). In addition, the results illustrate that the solution time in this case is much longer compared to case 1 (deterministic condition), which is due to the

consideration of uncertainties in this case. Fig. 16 indicates the voltage magnitude at 20 hour (peak hour) by a box plot diagram. As this figure shows, the voltage has always been within the allowable range in all scenarios.

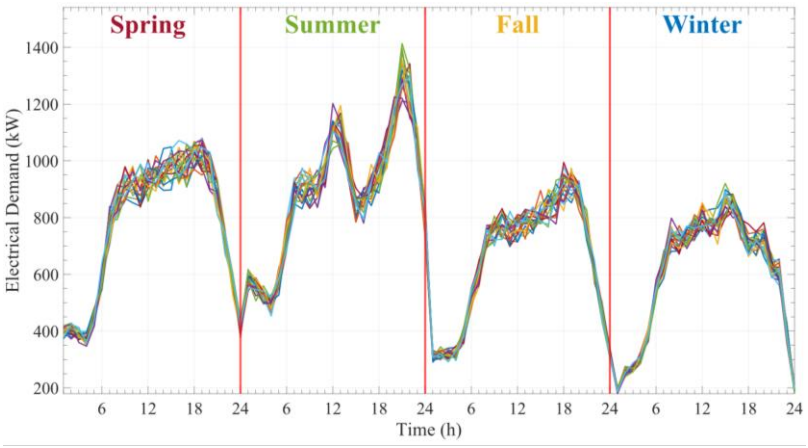

(a)

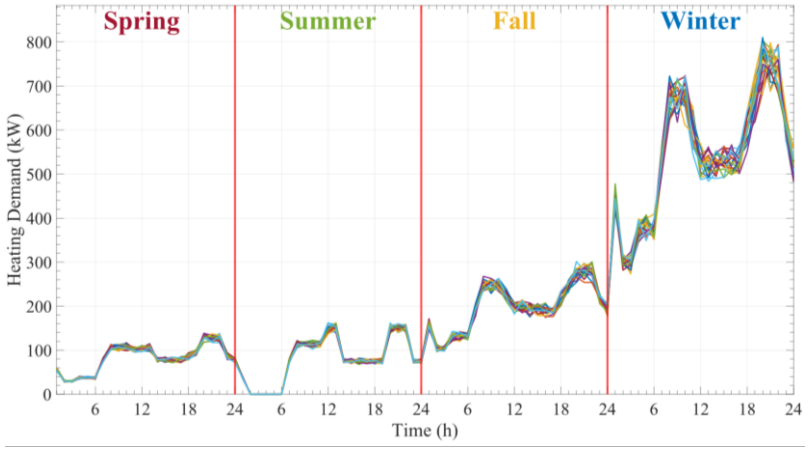

(b)

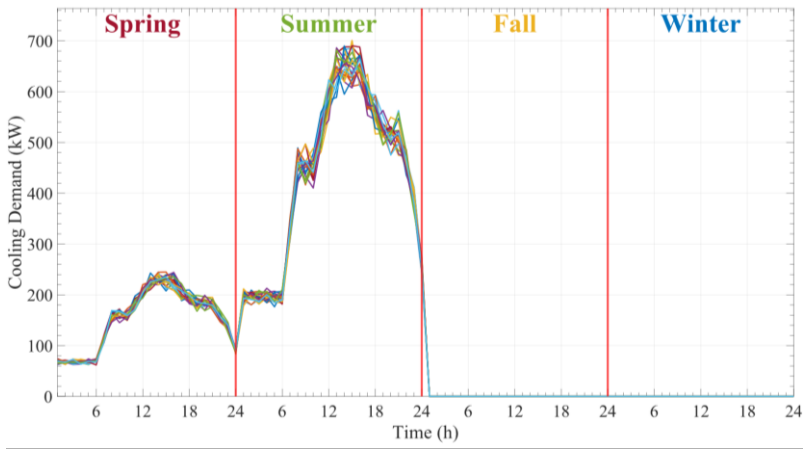

(c)

Fig. 12. (a) Electrical demand of residential hub; (b) Heating demand of residential hub; (c) Cooling demand of residential hub.

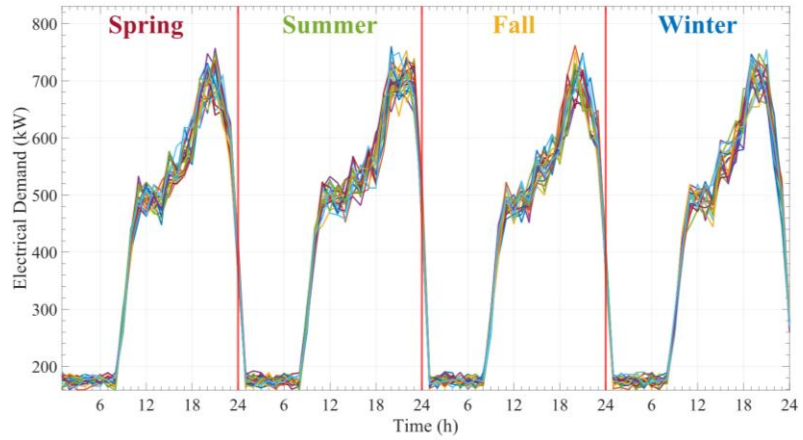

(a)

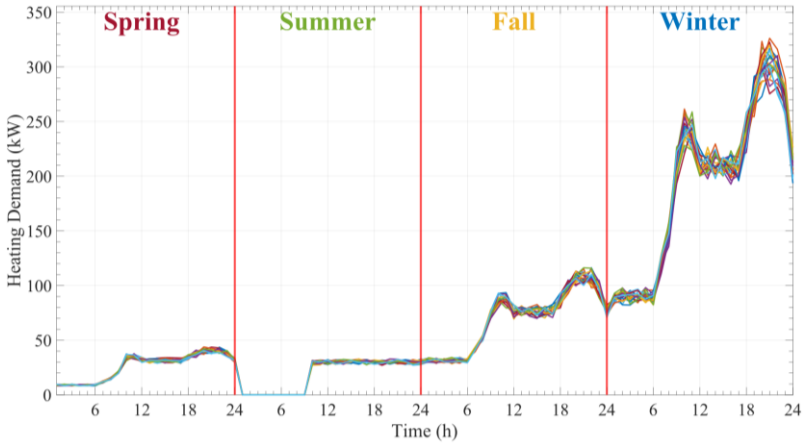

(b)

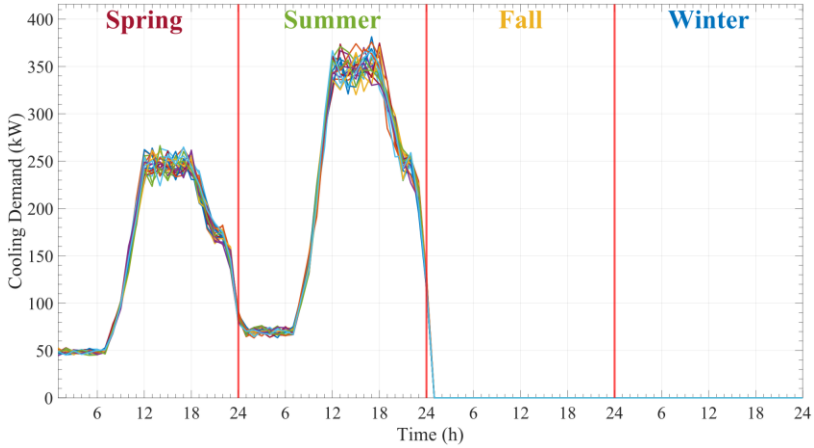

(c)

Fig. 13. (a) Electrical demand of commercial hub; (b) Heating demand of commercial hub; (c) Cooling demand of commercial hub.

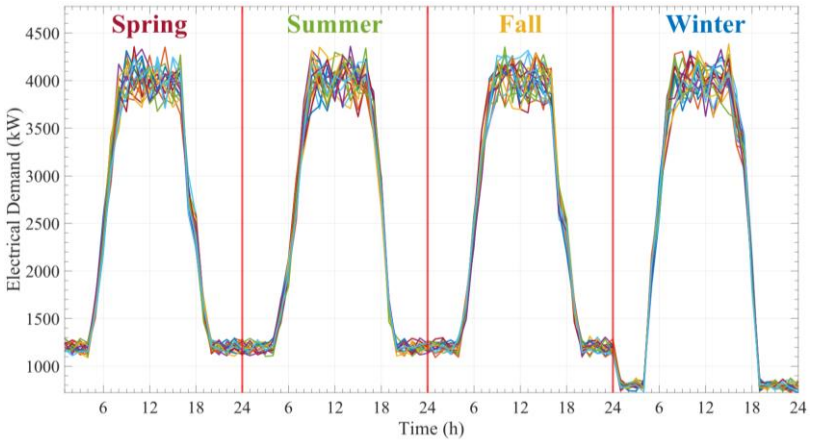

(a)

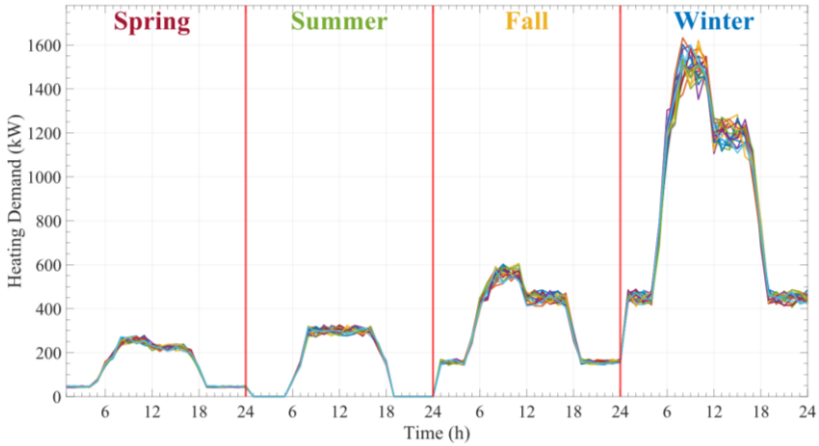

(b)

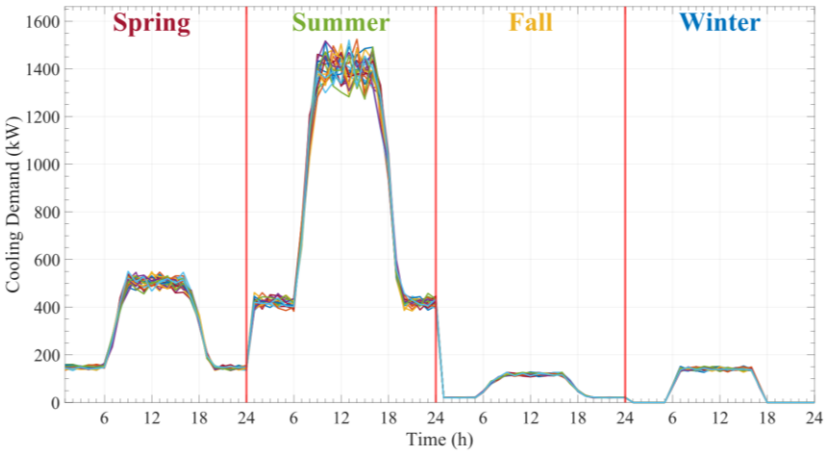

(c)

Fig. 14. (a) Electrical demand of industrial hub; (b) Heating demand of industrial hub; (c) Cooling demand of industrial hub.

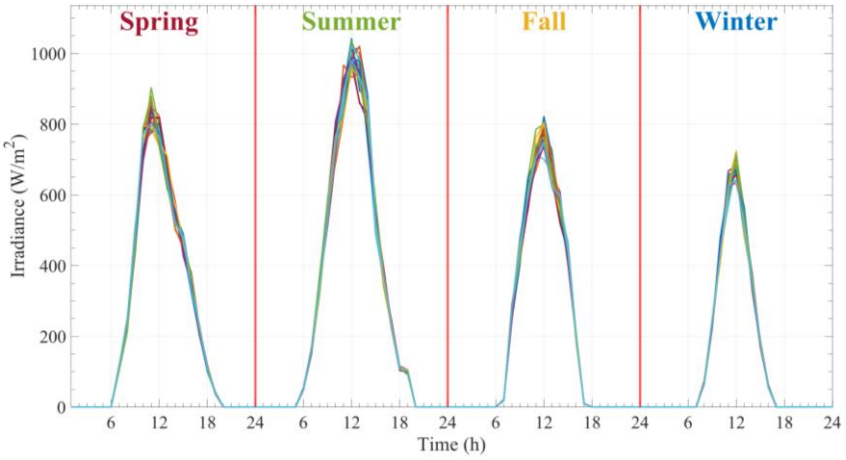

(a)

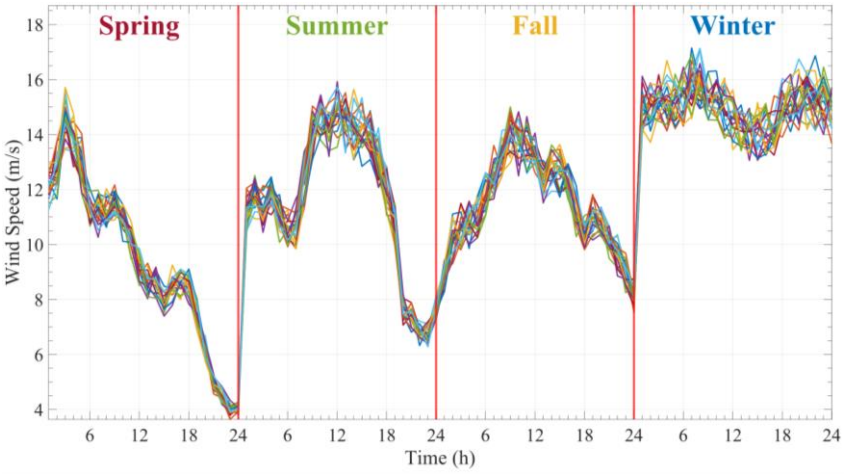

(b)

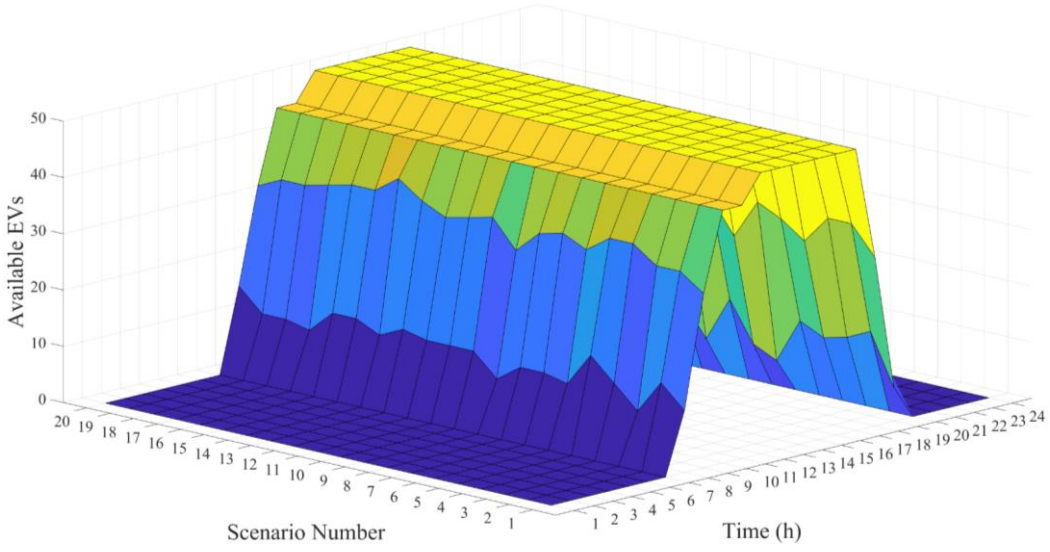

(c)

Fig. 15. (a) Solar irradiation; (b) Wind speed; (c) EVs availability.

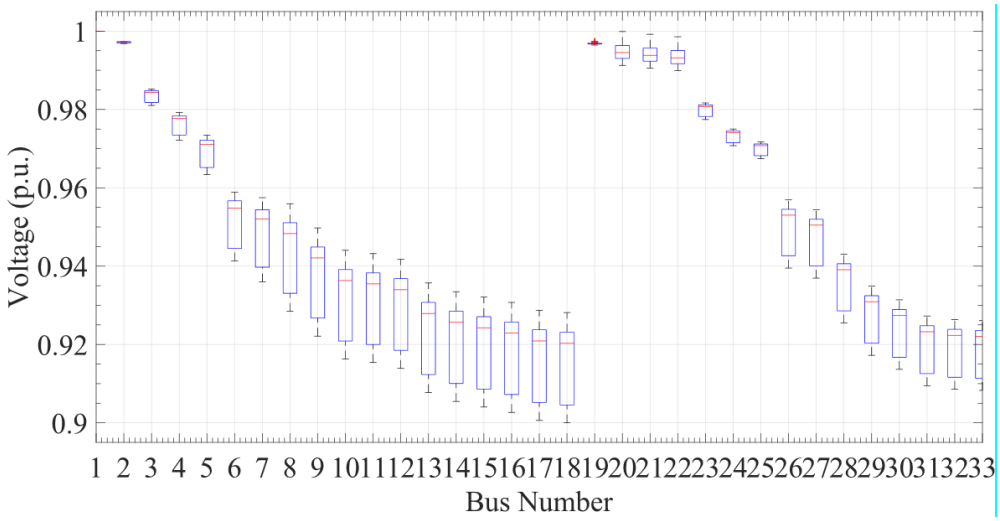

Fig. 16. The voltage magnitude of each bus at 20:00 h in summer: Case 2

Table 7. The annual costs of coordinated and uncoordinated operation modes: Case 2.

Type of Energy Hubs	Operating Mode					
	Coordinated			Uncoordinated		
	OC ($)	Buy ($)	Sell ($)	OC ($)	Buy ($)	Sell ($)
Industrial	4351057.48	699027.89	86287.71	5310549.4	678258.25	0
Commercial	417096.69	99208.61	33208.38	439266.99	73363.91	0
Residential	546947.16	140851.46	1695.82	610358.13	136307.88	0
Convergence Time (sec)		389.718			257.57	

5-3- Contingent events

This section evaluates the performance of the coordinated operation mode in supplying the load demand during contingencies. It is noteworthy that the industrial load is the vital load, therefore, maintaining the load of the industrial load has the first merit of order. The hub operators' main responsibility is to serve the industrial loads during the contingent event. In other words, the cost of energy not served for the industrial load is much higher than commercial and residential loads. In this regard, two case studies are investigated where the connection to the upstream grid is lost at two different periods of a given day in summer.

5-3-1- Event 1

In this case, the connection to the upstream grid would be lost between hours 10-12 of a given day in summer. It is noteworthy that the load demand of the industrial units is at the maximum value.

Figs. 17(a) and 17(b) indicate the value of the ENS in percent, relating to each hub and taking into account the coordinated and uncoordinated operation modes. As Fig. 17(a) shows, the three energy hubs would not be able to supply a fraction of their load demand in the uncoordinated operation mode. This issue will lead to the load curtailment in the residential and commercial energy hubs and also stopping production in the industrial hub which is not acceptable. On the other hand, using the coordinated operation mode would result in zero load curtailment in the industrial energy hub as shown in Fig. 17(b).

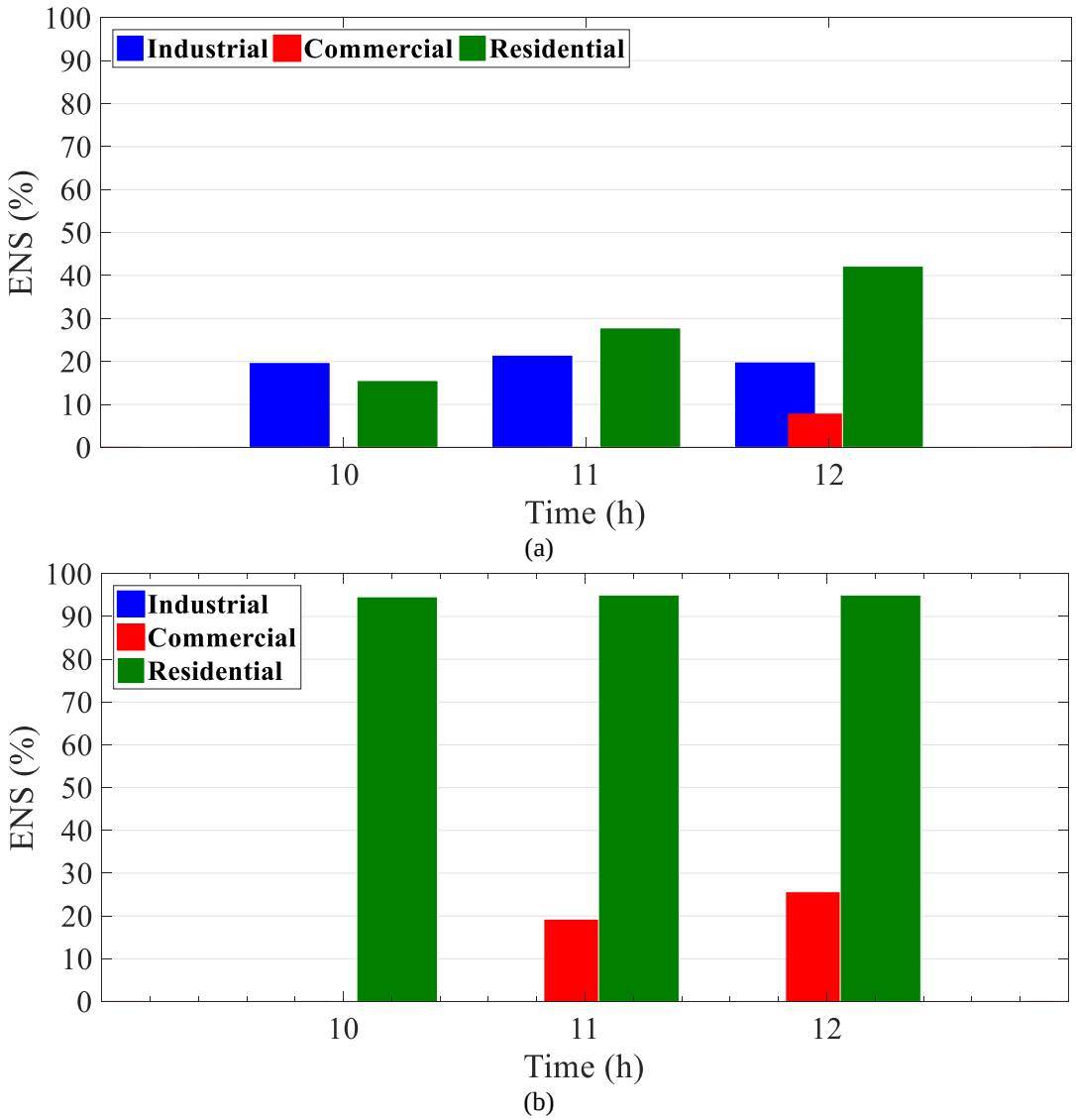

Fig. 17. (a) ENS in the uncoordinated operation mode; (b) ENS in the coordinated operation mode.

This is due to the higher significance of the industrial hub's load demand. In this regard, the residential and commercial hubs contribute to delivering power to the industrial hub to avoid any load curtailment. However, the value of ENS increases in the residential and commercial hubs in the coordinated operation, which is rational with respect to the higher importance of the industrial hub compared to other hubs.

5-3-2- Event 2

In this case, the hub is disconnected from the upstream grid during hours 21-23 of a given day in summer. It is noted that the load demand of the residential and commercial hubs is at the maximum value. As Fig. 18 depicts, a large fraction of the load demand is curtailed in these two hubs using the uncoordinated operation mode. However, the industrial hub would not face any load curtailment due to its relatively low load demand over this period. On the contrary, using the coordinated operation would result in no load curtailment. In this respect, the load demand of the industrial hub is low. Accordingly, the available capacity of the CHP unit in this hub can be utilized to deliver power to the residential and commercial hubs.

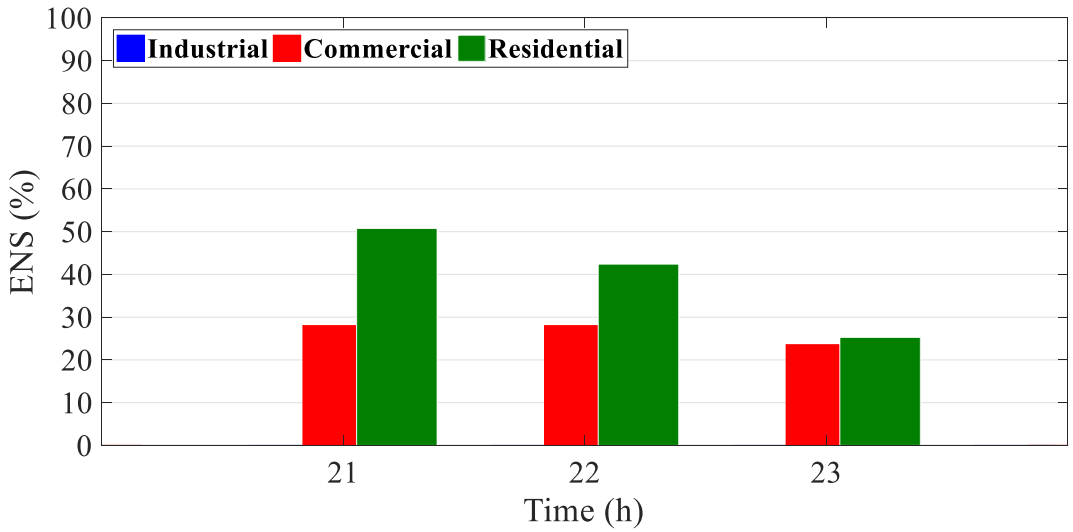

Fig. 18. ENS in the uncoordinated operation mode

6- Conclusion

This paper investigated the coordinated and uncoordinated operation models for multiple energy hubs, connected to a radial distribution system. The seasonal data of the load demand, price and renewable power generation were used to obtain a model close-to-real operation conditions.

Besides, the network configuration and ACOPF constraints were considered to avoid any unreal power transaction. The simulation results showed that the operating cost was significantly lower using the coordinated operation mode. Furthermore, the emission cost of the hubs and the system's power losses also reduced, mainly due to the lower amount of power purchased from the upstream grid in the coordinated operation. Applying the price-based DRP led to mitigating the operating cost, achieved by shifting the peak load demand to off-peak hours. Finally, the performance of the two operation models was assessed during contingencies and disconnection from the upstream grid. The results obtained verify the superiority of the coordinated operation by zero load curtailment in the industrial energy hub.

Acknowledgement

J.P.S. Catalão acknowledges the support by FEDER funds through COMPETE 2020 and by Portuguese funds through FCT, under POCI-01-0145-FEDER-029803 (02/SAICT/2017).

References

[1] Geidl M, Andersson G. Optimal Power Flow of Multiple Energy Carriers. IEEE Trans Power Syst 2007;22:145–55. https://doi.org/10.1109/TPWRS.2006.888988.

[2] Fang J. Dynamic Optimal Energy Flow in the Integrated Natural Gas and Electrical Power Systems. 2018 IEEE Power Energy Soc. Gen. Meet., 2018, p. 1. https://doi.org/10.1109/PESGM.2018.8586246.

[3] Zhang Y, Campana PE, Yang Y, Stridh B, Lundblad A, Yan J. Energy flexibility from the consumer: Integrating local electricity and heat supplies in a building. Appl Energy 2018;223:430–42. https://doi.org/https://doi.org/10.1016/j.apenergy.2018.04.041.

[4] Mansouri SA, Javadi MS. A robust optimisation framework in composite generation and transmission expansion planning considering inherent uncertainties. J Exp Theor Artif Intell 2017;29:717–30. https://doi.org/10.1080/0952813X.2016.1259262.

[5] Javadi MS, Esmaeel Nezhad A. Multi-objective, multi-year dynamic generation and transmission expansion planning- renewable energy sources integration for Iran's National Power Grid. Int Trans Electr Energy Syst 2019;29. https://doi.org/10.1002/etep.2810.

[6] Fotuhi-Firuzabad M. Day-ahead energy management framework for a networked gas–heat–electricity microgrid. IET Gener Transm Distrib 2019;13:4617-4629(12).

[7] Maroufmashat A, Elkamel A, Fowler M, Sattari S, Roshandel R, Hajimiragha A, et al. Modeling and optimization of a network of energy hubs to improve economic and emission considerations. Energy 2015;93:2546–58. https://doi.org/https://doi.org/10.1016/j.energy.2015.10.079.

[8] Sheikhi A, Rayati M, Ranjbar AM. Energy Hub optimal sizing in the smart grid; machine

learning approach. 2015 IEEE Power Energy Soc. Innov. Smart Grid Technol. Conf., 2015, p. 1–5. https://doi.org/10.1109/ISGT.2015.7131796.

[9] Ghorab M. Energy hubs optimization for smart energy network system to minimize economic and environmental impact at Canadian community. Appl Therm Eng 2019;151:214–30. https://doi.org/https://doi.org/10.1016/j.applthermaleng.2019.01.107.

[10] Zhou L, Liu N, Zhang Y. Energy Management for Smart Energy Hub Considering Gas Dispatch Factor and Demand Response. 2018 2nd IEEE Conf. Energy Internet Energy Syst. Integr., 2018, p. 1–6. https://doi.org/10.1109/EI2.2018.8582162.

[11] Chamandoust H, Derakhshan G, Hakimi SM, Bahramara S. Tri-objective optimal scheduling of smart energy hub system with schedulable loads. J Clean Prod 2019;236:117584. https://doi.org/https://doi.org/10.1016/j.jclepro.2019.07.059.

[12] Gholinejad HR, Loni A, Adabi J, Marzband M. A hierarchical energy management system for multiple home energy hubs in neighborhood grids. J Build Eng 2020;28:101028. https://doi.org/https://doi.org/10.1016/j.jobe.2019.101028.

[13] Roustai M, Rayati M, Sheikhi A, Ranjbar AM. A scenario-based optimization of Smart Energy Hub operation in a stochastic environment using conditional-value-at-risk. Sustain Cities Soc 2018;39:309–16. https://doi.org/10.1016/j.scs.2018.01.045.

[14] Ghazvini MAF, Steen D, Tuan LA. A Centralized Building Energy Management System for Residential Energy Hubs. 2019 Int. Conf. Smart Energy Syst. Technol., 2019, p. 1–6. https://doi.org/10.1109/SEST.2019.8849066.

[15] Javadi MS, Nezhad AE, Nardelli PHJ, Gough M, Lotfi M, Santos S, et al. Self-scheduling model for home energy management systems considering the end-users discomfort index within price-based demand response programs. Sustain Cities Soc 2021;68:102792. https://doi.org/10.1016/j.scs.2021.102792.

[16] Wang J, Zhong H, Ma Z, Xia Q, Kang C. Review and prospect of integrated demand response in the multi-energy system. Appl Energy 2017;202:772–82. https://doi.org/https://doi.org/10.1016/j.apenergy.2017.05.150.

[17] Sheikhi A, Rayati M, Bahrami S, Ranjbar AM. Integrated Demand Side Management Game in Smart Energy Hubs. IEEE Trans Smart Grid 2015;6:675–83. https://doi.org/10.1109/TSG.2014.2377020.

[18] Chamandoust H, Derakhshan G, Hakimi SM, Bahramara S. Tri-objective scheduling of residential smart electrical distribution grids with optimal joint of responsive loads with renewable energy sources. J Energy Storage 2020;27:101112. https://doi.org/https://doi.org/10.1016/j.est.2019.101112.

[19] Jadidbonab M, Babaei E, Mohammadi-ivatloo B. CVaR-constrained scheduling strategy for smart multi carrier energy hub considering demand response and compressed air energy storage. Energy 2019;174:1238–50. https://doi.org/https://doi.org/10.1016/j.energy.2019.02.048.

[20] Gholizadeh N, Gharehpetian GB, Abedi M, Nafisi H, Marzband M. An innovative energy management framework for cooperative operation management of electricity and natural gas demands. Energy Convers Manag 2019;200:112069.

https://doi.org/https://doi.org/10.1016/j.enconman.2019.112069.

[21] Zhou S, Zou F, Wu Z, Gu W, Hong Q, Booth C. A smart community energy management scheme considering user dominated demand side response and P2P trading. Int J Electr Power Energy Syst 2020;114:105378. https://doi.org/https://doi.org/10.1016/j.ijepes.2019.105378.

[22] Coelho A, Neyestani N, Soares F, Lopes JP. Wind variability mitigation using multi-energy systems. Int J Electr Power Energy Syst 2020;118:105755. https://doi.org/https://doi.org/10.1016/j.ijepes.2019.105755.

[23] Korkas CD, Baldi S, Michailidis I, Kosmatopoulos EB. Occupancy-based demand response and thermal comfort optimization in microgrids with renewable energy sources and energy storage. Appl Energy 2016;163:93–104. https://doi.org/10.1016/j.apenergy.2015.10.140.

[24] Tavakoli M, Shokridehaki F, Funsho Akorede M, Marzband M, Vechiu I, Pouresmaeil E. CVaR-based energy management scheme for optimal resilience and operational cost in commercial building microgrids. Int J Electr Power Energy Syst 2018;100:1–9. https://doi.org/10.1016/j.ijepes.2018.02.022.

[25] Korkas CD, Baldi S, Kosmatopoulos EB. Grid-Connected Microgrids: Demand Management via Distributed Control and Human-in-the-Loop Optimization. Adv. Renew. Energies Power Technol., vol. 2, Elsevier; 2018, p. 315–44. https://doi.org/10.1016/B978-0-12-813185-5.00025-5.

[26] Tavakoli M, Shokridehaki F, Marzband M, Godina R, Pouresmaeil E. A two stage hierarchical control approach for the optimal energy management in commercial building microgrids based on local wind power and PEVs. Sustain Cities Soc 2018;41:332–40. https://doi.org/10.1016/j.scs.2018.05.035.

[27] Javadi MS, Saniei M, Rajabi Mashhadi H. An augmented NSGA-II technique with virtual database to solve the composite generation and transmission expansion planning problem. J Exp Theor Artif Intell 2014;26. https://doi.org/10.1080/0952813X.2013.815280.

[28] Javadi, Sadegh M, Lotfi M, Nezhad AE, Anvari-Moghaddam A, Guerrero JM, et al. Optimal Operation of Energy Hubs Considering Uncertainties and Different Time Resolutions. IEEE Trans. Ind. Appl., vol. 56, Institute of Electrical and Electronics Engineers Inc.; 2020, p. 5543–52. https://doi.org/10.1109/TIA.2020.3000707.

[29] Javadi MS, Anvari-Moghaddam A, Guerrero JM, Esmaeel Nezhad A, Lotfi M, Catalao JPS. Optimal Operation of an Energy Hub in the Presence of Uncertainties. 2019 IEEE Int Conf Environ Electr Eng 2019 IEEE Ind Commer Power Syst Eur (EEEIC / I&CPS Eur 2019:1–4. https://doi.org/10.1109/EEEIC.2019.8783452.

[30] Javadi MS, Esmaeel Nezhad A, Sabramooz S. Economic heat and power dispatch in modern power system harmony search algorithm versus analytical solution. Sci Iran 2012;19. https://doi.org/10.1016/j.scient.2012.10.033.

[31] Razavi S-E, Javadi MS, Esmaeel Nezhad A. Mixed-integer nonlinear programming framework for combined heat and power units with nonconvex feasible operating region: Feasibility, optimality, and flexibility evaluation. Int Trans Electr Energy Syst 2019;29:1–18. https://doi.org/10.1002/etep.2767.

[32] Nezhad AE, Ghanavati F, Ahmarinejad A. Determining the Optimal Operating Point of CHP Units with Nonconvex Characteristics in the Context of Combined Heat and Power Scheduling Problem. IETE J Res 2020. https://doi.org/10.1080/03772063.2020.1724522.

[33] Javadi MS, Anvari-Moghaddam A, Guerrero JM. Optimal scheduling of a multi-carrier energy hub supplemented by battery energy storage systems. Conf. Proc. - 2017 17th IEEE Int. Conf. Environ. Electr. Eng. 2017 1st IEEE Ind. Commer. Power Syst. Eur. EEEIC / I CPS Eur. 2017, 2017. https://doi.org/10.1109/EEEIC.2017.7977520.

[34] Javadi MS, Anvari-Moghaddam A, Guerrero JM. Robust energy hub management using information gap decision theory. Proc. IECON 2017 - 43rd Annu. Conf. IEEE Ind. Electron. Soc., vol. 2017- Janua, 2017. https://doi.org/10.1109/IECON.2017.8216073.

[35] Simab M, Javadi MS, Nezhad AE. Multi-objective programming of pumped-hydro-thermal scheduling problem using normal boundary intersection and VIKOR. Energy 2018;143. https://doi.org/10.1016/j.energy.2017.09.144.

[36] Javadi MS, Lotfi M, Gough M, Nezhad AE, Santos SF, Catalao JPS. Optimal Spinning Reserve Allocation in Presence of Electrical Storage and Renewable Energy Sources. 2019 IEEE Int Conf Environ Electr Eng 2019 IEEE Ind Commer Power Syst Eur (EEEIC / I&CPS Eur 2019:1–6. https://doi.org/10.1109/EEEIC.2019.8783696.

[37] Mansouri SA, Ahmarinejad A, Ansarian M, Javadi MS, Catalao JPS. Stochastic planning and operation of energy hubs considering demand response programs using Benders decomposition approach. Int J Electr Power Energy Syst 2020;120:106030. https://doi.org/10.1016/j.ijepes.2020.106030.

[38] Mansouri SA, Ahmarinejad A, Javadi MS, Nezhad AE, Shafie-Khah M, Catalão JPS. Chapter 9 - Demand response role for enhancing the flexibility of local energy systems. In: Graditi G, Di Somma MBT-DER in LIES, editors., Elsevier; 2021, p. 279–313. https://doi.org/https://doi.org/10.1016/B978-0-12-823899-8.00011-X.

[39] Javadi MS, Azami R, Monsef H. Security constrained unit commitment of interconnected power systems. Int Rev Electr Eng 2009;4.

[40] Mansouri SA, Ahmarinejad A, Javadi MS, Catalão JPS. Two-stage stochastic framework for energy hubs planning considering demand response programs. Energy 2020:118124. https://doi.org/10.1016/j.energy.2020.118124.

[41] Javadi MS, Esmaeel Nezhad A, Siano P, Shafie-khah M, Catalão JPS. Shunt capacitor placement in radial distribution networks considering switching transients decision making approach. Int J Electr Power Energy Syst 2017;92. https://doi.org/10.1016/j.ijepes.2017.05.001.

[42] Estahbanati MJ. Hybrid probabilistic-harmony search algorithm methodology in generation scheduling problem. J Exp Theor Artif Intell 2014;26:283–96. https://doi.org/10.1080/0952813X.2013.861876.

[43] Liang H, Liu Y, Li F, Shen Y. A multiobjective hybrid bat algorithm for combined economic/emission dispatch. Int J Electr Power Energy Syst 2018;101:103–15. https://doi.org/10.1016/j.ijepes.2018.03.019.

[44] Khorshid-Ghazani B, Seyedi H, Mohammadi-Ivatloo B, Zare K, Shargh S. Reconfiguration

of distribution networks considering coordination of the protective devices. IET Gener Transm Distrib 2017;11:82–92. https://doi.org/10.1049/iet-gtd.2016.0539.

[45] Pazouki S, Haghifam MR, Moser A. Uncertainty modeling in optimal operation of energy hub in presence of wind, storage and demand response. Int J Electr Power Energy Syst 2014;61:335–45. https://doi.org/10.1016/j.ijepes.2014.03.038.